Surface Science 199 (1988) 320–360
North-Holland, Amsterdam

THIOPHENE HYDRODESULFURIZATION ON MoS_2; THEORETICAL ASPECTS

Marjanne C. ZONNEVYLLE, Roald HOFFMANN *

Department of Chemistry and Materials Science Center, Cornell University, Ithaca, NY 14853-1301, USA

and

Suzanne HARRIS

Exxon Research and Engineering Co., Route 22 East, Clinton Township, Annandale, NJ 08801, USA

Received 4 September 1987; accepted for publication 21 December 1987

Hydrodesulfurization (HDS), the removal of sulfur in the form of H_2S from petroleum, is a crucial step in the industrial refinement process. Using the extended Hückel tight binding method, we have examined the nature of the active site and the mechanism of desulfurization in the case of thiophene on MoS_2. The η^5-bound sites, in which the thiophene ring lies parallel to the surface, are particularly advantageous to weakening the S–C bond. η^1-bound sites are less active. The removal of surrounding surface sulfurs increases the HDS potential of the η^5 geometry, but is ineffective at promoting the poorer adsorption modes. Surface reconstruction has also been examined; the possibility of Mo–Mo pairing is suggested. The effect of poisons and promoters is considered. The role they play in HDS catalysis may be determined by the position they occupy in the MoS_2 lattice. Metals which replace a surface molybdenum tend to poison HDS, whereas those which "pseudo-intercalate" between the S–S layers can serve to promote the reaction.

1. Introduction

Catalytic hydrodesulfurization (HDS) is a vital step in the processing of petroleum into useful hydrocarbon products [1]. Petroleum carries many sulfur-containing compounds, which must be converted into desulfurized organics and H_2S waste before use. For the light (low molecular weight) fractions, the concern is that sulfur will reduce the stability of the product fuels and will poison the platinum based catalysts used for their combustion. The heavy (high molecular weight) fractions are converted into jet and heating fuels; for these, the reduction of SO_2 pollution motivates the cleansing.

Both aromatic and nonaromatic organosulfur compounds are found in petroleum. The nonaromatic thiols, sulfides and disulfides readily undergo hydrodesulfurization. Much less reactive are the aromatic species. These are

0039-6028/88/$03.50

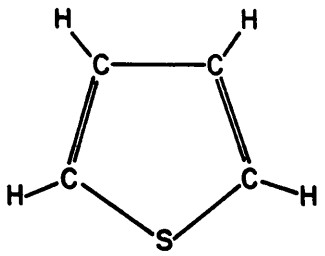

Scheme 1

comprised largely of thiophene, dibenzothiophene and other thiophenic species. Thiophene, SC_4H_4 (scheme 1), is a 5-membered planar ring and is the simplest aromatic in the feedstock. Under catalytic HDS conditions, it yields primarily butane (C_4H_{10}) although some lighter hydrocarbon products are observed due to hydrocracking. If the reaction is performed under low H_2 pressures, the main product is butadiene (C_4H_6). It is unknown whether desulfurization or hydrogenation of the thiophene ring occurs first, or if the process is concerted. In the case of dibenzothiophene, however, it is known that desulfurization tends to occur first [1b]. Of the two steps, desulfurization is the more crucial, as hydrogenation can occur under a great variety of different catalytic conditions but desulfurization is nearly specific to the transition metal dichalcogenides. Thus, it is important to stress that desulfurization can occur without full prior hydrogenation.

Catalysts based on the layered transition metal dichalcogenides are historically the most widely used industrial HDS catalysts. These usually contain some combination of Co, Ni, Mo and W sulfides. The morphology of the mixed phases, such as the very active Co/Mo/S phase, is a subject of some speculation, which we will consider later. The industrial catalyst are small, porous sulfided crystallites bound to an Al_2O_3 or silica–alumina support. There were early suggestions that the alumina carrier could be catalytically active and, in particular, performed a crucial role in promotion [1a,3]. But as both unsupported sulfides [2a] and carbon supported sulfides [2b] can catalyze HDS, the catalytic activity appears to arise from the sulfide itself rather than the support.

Much of the recent theoretical and experimental work in HDS has concentrated specifically on the process of S–C bond cleavage in thiophene on MoS_2. Still, many factors, such as the initial adsorption geometry, the identity of the active site and a workable model for the reaction mechanism are obscure. The crucial experiments remain difficult to conduct because of the highly anisotropic morphology of MoS_2. The theoretical work has been hampered by the complexity of the system. We shall propose several possible active sites for thiophene HDS on MoS_2, and address the problems of defects, surface reconstruction and promoters.

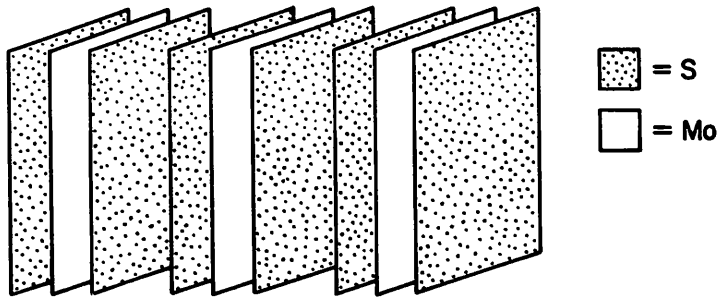

Scheme 2

MoS_2 forms a layered structure; hexagonal S and Mo nets are stacked to give S–Mo–S "sandwiches", scheme 2. Inside the sandwiches, each molybdenum is coordinated in a trigonal prismatic fashion by six sulfur atoms. The sandwiches are stacked to create close packing contacts between the sulfur layers. A cross section of three adjacent sandwiches is shown in scheme 3. The intersandwich spacing of 3.16 Å indicates that the units are held together by van der Waals forces and thus are essentially isolated. The crystals cleave easily to expose the all sulfur basal plane (002). This is *not*, however, the active surface. Essentially it is a plane of sulfur lone pairs, and thus predictably inert to adsorption and reactions. Neither thiophene, 1,3-butadiene nor H_2S decompose on the basal plane [4].

According to several recent studies, the active surface exposes molybdenum centers. By cutting the crystals perpendicular to the natural cleavage plane, the activities of the basal and Mo-containing surfaces can be compared directly. The rate of catalytic olefin isomerization increases with the amount of cut surface exposed [5]. HDS activity can be correlated to the number of Mo centers on the surface as measured by the extent of oxygen chemisorption [6], ESR spin density [7], and magnetic susceptibility [8]. By exploiting the relationship between crystal size and the relative numbers of edge, corner and

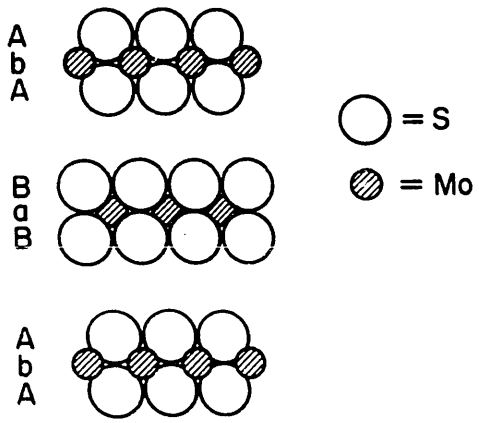

Scheme 3

basal sites, it was forwarded that HDS, hydrogenation and O_2 chemisorption data was best fit to a model which requires that the edge sites are the only active sites [9]. No correlation is found between HDS activity and the BET surface area [6], which is a measure of the total surface area [10].

A commonly called upon model for the active surface is the (100) edge plane, a side view of which is shown in scheme 3. A perfect (100) surface is physically very difficult to create, because the anisotropy of the MoS_2 architecture lends itself to growing very thin crystals with large basal planes. In addition, the majority of the exposed Mo in scheme 3 are likely to be "tied-off" with an additional layer of sulfur. Several investigators have advocated that catalytic HDS occurs at defect sites in the edge plane and corner sites along the edge–basal junction [11]. There is some experimental evidence that olefin isomerization and hydrogenation occur at coordinatively unsaturated sites [5]. The defect density on single crystal MoS_2 platelets as measured by optical absorbence can be correlated to the HDS of dibenzothiophene [12]. Even the inertness of the basal plane to O_2 chemisorption can be reversed by sputtering to create defects [13]. On the edge plane, a defect site may be formed, for example, by removing one or more surface sulfur atoms. This type of defect, as well as the corner sites, will expose an unsaturated Mo center. Intuitively, these sites could offer a particularly attractive coordination environment for adsorbates, and may have an elevated chemical activity when compared to sites on the pristine edge plane.

Much of the analysis of the HDS active site can be performed on MoS_2 directly. Thus far, single crystal studies, which are necessary to understanding the mechanistic details of the catalytic process, have not been performed on the active edge plane because of the difficulty in obtaining single crystals with enough edge plane area to study. The reaction must be examined by less direct routes. There are three typical approaches: (1) reactor modeling under catalytic condition, (2) extrapolation from molecular organometallic analogues, and (3) examination of thiophene (or thiophenic species) on clean transition metal surfaces. The first was paramount in the identification of the Mo-exposing surface as the active surface [5,6]. The method has also been used to elucidate the role of promoters, as we will discuss later.

Many investigators have chosen to model the HDS system with thiophene or other organosulfur adsorbates on well characterized, clean transition metal surfaces. Thiophene decomposes to atomic surface S and C, and gaseous H_2 on some surfaces such as Mo(110) [14]. Unless the reaction can be slowed down, as was reported in this case with the preadsorption of atomic sulfur, these are relatively uninformative surfaces as HDS analogues. If molecular thiophene chemisorption does occur, the initial adsorption geometry and the HDS active geometry (the two need not be identical) appear to be highly surface and, in some cases, coverage dependent. Some schemes propose a shift from the adsorption to the active geometry with increasing temperature and

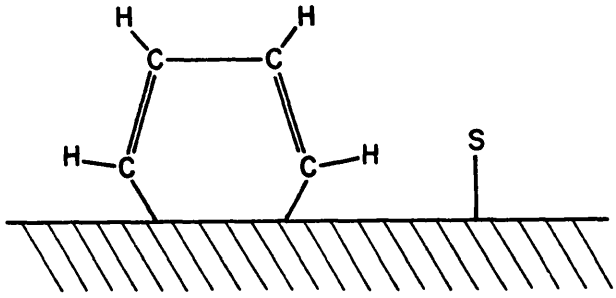

Scheme 4

prior to any S–C bond scission. For example, on Pt(111) at 180 K, a shift is proposed from an inactive ~ 40° cant of the ring to the surface, to the active geometry which places the ring parallel to the surface [15]. The coordination through all five ring atoms makes particularly good use of the thiophene π system, as we will show later. Paralleling organometallic nomenclature, it can be called an η^5-bound species. In contrast to the (111) face, the shift on the Pt(100) surface is in the opposite direction, from parallel to tilted [16]. No shift is proposed on Ni(100); the active species is imagined bound through the sulfur and perpendicular to the surface [17]. The two lone pairs of the sulfur will be important to this η^1-coordination mode. On Mo(100), the active geometry is coverage dependent – parallel at low coverages with an alternate perpendicular geometry available at high coverages [18].

At higher temperatures, the S–C bond cleaves to yield chemisorbed atomic sulfur and a surface hydrocarbon species. Although the evidence in many cases does not necessarily preclude other structures, the surface fragment is often visualized as a metallocycle. Proposed are either MC_4H_4, scheme 4, or the partially dehydrogenated MC_4H_3 or MC_4H_2. During the course of a single study on a wide range of metal surfaces, metallocyclic intermediates were strongly favored for Ni(100), Ru(001) and Os(001), and less strongly favored for Ni(111), Ir(111) Pt(111), Pd(100) and Pd(111) [19].

Dehydrogenation of the hydrocarbon occurs at higher temperatures to produce surface atomic C and hydrogen gas. Recall that catalytic HDS intermediates undergo hydrogenation, rather than dehydrogenation. Hydrogenation cannot occur under ultrahigh vacuum conditions, but the important point is that desulfurization can occur prior to hydrogenation. All in all, it may be easier to cleave the S–C bond in saturated species. For example, if one of the six-membered rings of dibenzothiophene is saturated, HDS becomes much more facile than for dibenzothiophene itself [1b]. On several Pt surfaces, under similar conditions, the S–C bond scission in tetrahydrothiophene (SC_4H_8, the saturated analogue of thiophene) will occur at temperatures as much as 150 K lower than for thiophene. The proposed intermediate for the tetrahydrothiophene reaction is a potentially aromatic sulfur containing metal-

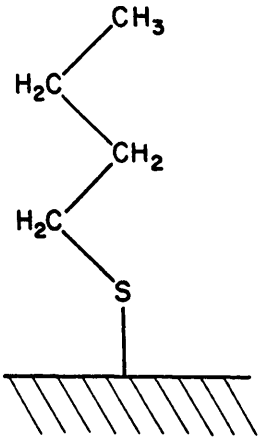

Scheme 5

locycle, MS_4H_4 [16]. Sulfur containing metallocyclic intermediates have not yet been suggested for thiophene decomposition. An intriguing noncyclic intermediate, the butyl thiolate SC_4H_9, scheme 5 has been proposed for the tetrahydrothiophene decomposition on Mo(110) [20]. The intermediate points to the possibility of a two step desulfurization in which the two S–C bonds are broken independently. The first S–C bond scission to produce scheme 5 may occur via an η^2 species bound through the sulfur and one adjacent α-carbon. The second scission can then proceed from the linear surface species. Other mechanisms imply a concerted replacement of the S by a metal atom, with little distortion of the cyclic character of the adsorbate.

Two binding modes have been observed for the handful of molecular organometallic species with thiophene ligands: η^1 bound through the sulfur end and η^5 bound through the 5 atoms of the ring. The η^1 complexes, such as $(NH_3)_5Ru(\eta^1\text{-}SC_4H_4)^{2+}$ [21a] and $Cp(CO)_2Fe(\eta^1\text{-}SC_4H_4)^+$ [21b] (Cp = cyclopentadiene, C_5H_5) are rare and are inert to HDS-like reactions. The metal–sulfur bond is weak and neither ring opening, desulfurization, nor hydrogen exchange has been observed [21]. Somewhat more common is η^5 coordination in compounds such as $(CO)_3Cr(\eta^5\text{-}SC_4H_4)$ [22a], $(CO)_3Mn(\eta^5\text{-}SC_4H_4)^+$ [22b] and $CpM(\eta^5\text{-}SC_4H_4)^{n+}$ (M = Fe, $n = 1$ [22a]; M = Ru, $n = 1$ [22d]; M = Rh, Ir, $n = 2$ [22e]). A series of detailed studies on several of the π-bound species has uncovered a reactivity proposed to be analogous to HDS. Hydrogen exchange can occur at the α position in $CpRu(\eta^5\text{-}SC_4H_4)^+$ [22d]. Both the ruthenium complex and $(CO)_3Mn(\eta^5\text{-}SC_4H_4)^+$ are active toward nucleophilic attack at the α position by species such as H^-, OCH_3^- or $SC_2H_5^-$ [23a–23c]. The ruthenium hydride adduct, when treated with an excess of donor ligands (dppe, $((C_6H_5)_2PCH_2)_2$, in benzene), will undergo ring scission [23a]. X-ray crystal structure analysis confirms the formation of the butadiene thiolate ligand [23d]. In light of this reactivity, it has been proposed that η^5 coordination is more likely to be HDS active.

Several theoretical studies have been undertaken to model both the adsorption and active sites. Due to the complexity of the HDS system, some of the approximations and simplifications have necessarily been severe. In an early simple Hückel and CNDO/2 study, a proton serves to represent the electron accepting surface for thiophene adsorption [24a]. Other investigators have used the extended Hückel method to consider the adsorption of H_2S onto one- and two-molybdenum clusters, favoring coordination to two metal centers [24b]. More recently, the same method was applied to $MoS_3H_3^+$ clusters to suggest perpendicular η^1 over parallel η^5 adsorption geometries [24c]. An extensive SCF-Xα study of the periodic trends found in transition metal sulfides proposes a dependence of the activity on both the filling of the highest occupied molecular orbital of a MS_6^{n-} cluster model and on the degree of covalency in the metal–sulfur bond. Based on these results, a model was suggested in which thiophenic molecules bind to the catalyst surface in an η^1 geometry at a sulfur vacancy. Backdonation of the metal electrons into a thiophenic π^* orbital could result in a weakening of the ring C–S bonds [25]. It has been suggested that HDS catalysts are hydrogenated in their active state and in his light, analysis of clusters of the type H_xMoS_2 finds that both Mo–H and S–H species may exist [26]. Other investigations has stressed the role of promoters in binary catalyst systems; we will discuss their contributions later.

Our calculations use the extended Hückel tight binding method [27] on an infinite system, rather than a cluster. The approximate MO method has well-documented deficiencies. For instance, it does not give the correct work functions or reliable potential energy curves. Binding energies can be compared only between similar sites, and little importance can be attached to their absolute values. We cannot identify the initial adsorption site nor follow the movement of adsorbates on the surface from an adsorption site to an active site. But we can analyze the basic orbital interactions governing each specific active site, particularly on a surface which is nonmagnetic, such as MoS_2. In terms of surface interactions, the system at hand, consisting of a large adsorbate interaction with a nonmetallic substrate, may be well suited to the method since the bonding will be dominated by covalent, rather than ionic, forces.

2. MoS_2 model

We will take the Mo exposing (100) edge plane of MoS_2 as the starting point for modeling the HDS active site. At the surface, one half of the metal atoms are coordinated to only four sulfurs, the remainder have the full trigonal prismatic compliment of six. Such a surface will probably not exist under catalytic conditions; many of the exposed Mo will be "tied-off" by extra sulfur

atoms (from reconstruction, or thiophene or H_2S decomposition). The fully coordinated Mo will serve as a model for the "pristine" surface, and the exposed Mo will act as the first and simplest of a series of defect site models.

The layered architecture of MoS_2 can be used to simplify the problem. The S–S layer spacing of 3.16 Å precludes significant interactions across the gap. Each S–Mo–S sandwich can then be treated as an independent unit. Three layers of the sandwich will form a one-dimensional infinite ribbon model. Two adjacent unit cells are shown in scheme 6. The single translational direction is along y (i.e., the unit cells are repeated infinitely in this direction). The top xy plane is the active edge face; Mo_3 and Mo_6 are protruding and four-coordinate. Similar two vacancy sites have been proposed as the active site for isomerization reactions [5]. The bottom xy plane acts as a pristine surface; Mo_9 and Mo_{12} are recessed and six-coordinate. Because of the stacking registry, the two types, which appear on opposite faces of the model crystal, are found on adjacent sandwiches of the edge plane for real MoS_2 crystals (see scheme 3). The yz plane is the inert all sulfur basal plane, and the z direction is perpendicular to the active edge face. To check the validity of the one-dimensional approach, a two-dimensional model was constructed as well. A second translational vector in the x direction is introduced, and an adjacent three layer sandwich must be added to the unit cells in scheme 6, so as to conserve the close packing contacts between the basal S layers. Comparison calculations between the two models, both with and without adsorbed thiophene, give close numerical agreement [28] and indicate parallel trends for the adsorption properties of thiophene. Unless specified otherwise, all further calculations use scheme 6. Computational details are presented in the appendix.

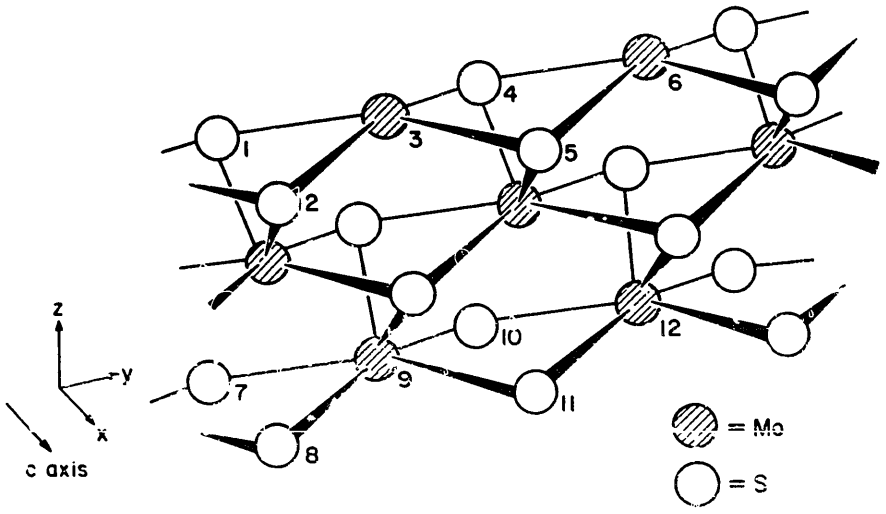

Scheme 6

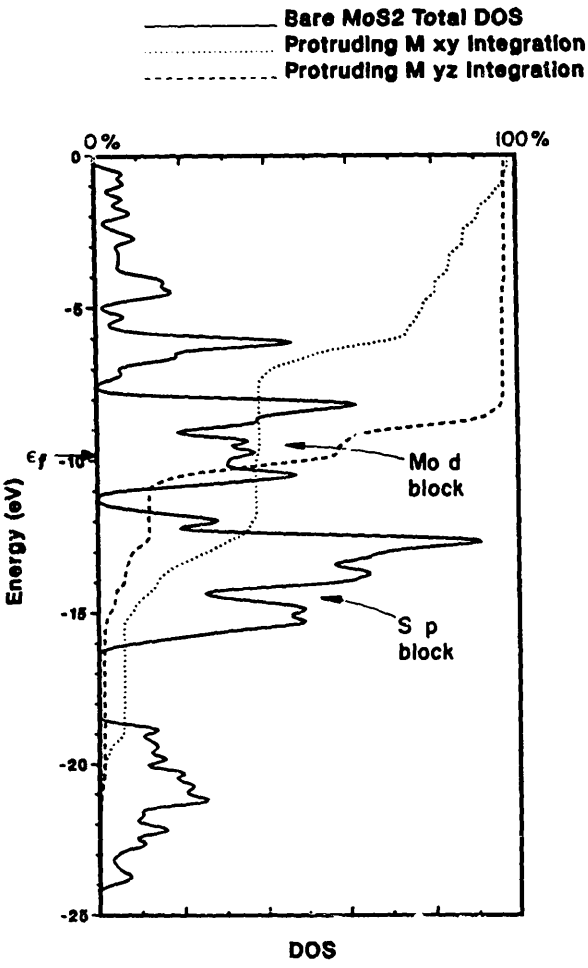

Fig. 1. The total DOS of the one-dimensional MoS_2 model (solid line) and the integrals of the protruding Mo *xy* (dotted line) and *yz* (dashed line).

Analysis of the electronic structure of the bare MoS_2 model, scheme 6, is fairly simple. The total density of state (DOS), the solid line in fig. 1, can be broken into four parts. From the bottom, we find the sulfur s levels (-24.0 to -18.5 eV), a large sulfur p block containing $\sim 80\%$ of the p levels (-16.2 to -11.3 eV), the more compact Mo d block (-11.0 to -7.5 eV) and the disperse Mo s and p levels (upwards from -11.0 eV). A detailed discussion of the electronic structure of the layered metal dichalcogenides may be found in an earlier paper from our group [29a]. The Fermi level falls in the d block. MoS_2 is known to be a semiconductor. Our calculation on the real three-dimensional geometry does give a gap of ~ 0.8 eV at ϵ_f. Electrical and optical measurements give a similar gap width [29b] and a ~ 0.7 eV gap is calculated by ab initio methods [29c]. A recent self-consistent calculation on the full MoS_2 structure found a slightly smaller gap [29d]. The gap disappears for scheme 6, not so much because of the one-dimensionality, but because one

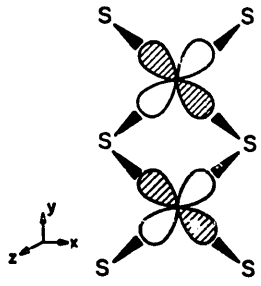

Scheme 7

third of the metals in the unit cell (those on the "protruding" surface) are coordinatively unsaturated. The d orbitals on these metals are not fully split into the Mo nonbonding levels in the valence band and Mo–S antibonding levels in the conduction band. As our arguments are not centered about conductivity, we believe that our analysis is nonetheless pertinent to the system. In fact, the open coordination sphere may favor stronger metal–metal interactions, as will be shown later.

The metal orbitals will play the leading role in interactions with a thiophene, so it is important to see their initial energy distribution. They can be followed by their projected density of states, i.e., their contribution to the total DOS. Alternatively, one can look at the integral of these contributions or projections. On a scale of 0–100% given at the top, these integrations specify the percentage of occupation of a specific atomic orbital at any energy. For instance, the dotted line in fig. 1 shows the integral of the Mo_3 xy levels. These orbitals point at the surface sulfur atoms, S_{surf}, as can be seen in the top view, scheme 7. Approximately 30% of the levels are pulled into the S p block to form the Mo–S bonds and their antibonding counterparts are pushed above the Mo d block. The interaction is so strong that we expect this level to be unaffected by adsorption of thiophene. The remaining d orbitals are the surface states which fill the gap. The yz orbitals are indicated in scheme 8. Their integral is shown as a dashed line in fig. 1. These orbitals protrude out of the surface and are essentially free to interact with adsorbate orbitals. The Mo–Mo interaction is responsible for the splitting of the yz levels about ϵ_f. An antibonding combination is drawn in scheme 8, and the splitting can be seen in the deflection of the integration line. The xz levels fall into a single sharp peak slightly above ϵ_f; the Mo–Mo δ interaction is weak. We will see

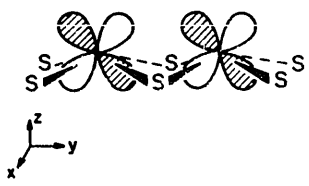

Scheme 8

that it are the *yz* orbitals which are crucial to thiophene adsorption at most sites.

Surface Mo_3 is reduced relative to the "bulk" Mo in the second layer. The net charges are +0.80 and +1.11 respectively. The observed electron gain by the surface Mo is consistent with calculations on MoS_2-like clusters [26]. Enhanced HDS activity might well be expected at reduced metal centers [30], as the donor strength into the empty thiophene levels can depend greatly on the electron density at the metal.

3. Thiophene

The aim of this work is to identify potential HDS active sites. It is imperative to stress that the initial adsorption site and active site need not be identical or even similar. The aforementioned shifts in the thiophene geometry as a function of temperature on various transition metal surfaces testify to this. Since we cannot reliably calculate a full potential surface for hydrodesulfurization we will touch only briefly on the question of the initial adsorption mode. For the same reason, we cannot directly identify the active site but must rely on indicators of what must be the essential component of the reaction coordinate, namely S–C bond weakening.

When such a bond weakening is observed, the computations allow, through a fragment analysis, a tracing of the bond weakening to the occupation of specific fragment orbitals. The occupation of such a fragment orbital in an infinite structure is found by assigning the atoms of the unit cell to one or more molecular fragments. The MO's of the fragments, rather than the atomic orbitals, can be used to form the basis set for the crystal wavefunction. We can decompose the total DOS in terms of this basis set as well, to obtain the projected DOS of fragment MO's.

The molecular orbitals of free thiophene are shown at the left in fig. 2. We see the typical cyclopentadienyl set of π orbitals, perturbed be the S heteroatom. Three of the π orbitals are filled. One of these, $2b_1$, is strongly localized on S, and can be called the S p or π type lone pair. The other, σ type lone pair on S is $9a_1$.

The only S–C antibonding orbital in the valence region is the lowest unoccupied molecular orbital (LUMO), $3b_1$, drawn in scheme 9. Partial population of $3b_1$ by interaction with the surface will cause weakening of the S–C bond. We will look for that occupation in our calculations. The assumption is that incipient S–C cleavage is signalled by $3b_1$ occupation. More complicated geometry changes, involving population of S–C σ^* orbitals must eventually follow for complete scission to occur.

Adsorption of simple diatomics is typically described according to the Blyholder model [31]. The chemisorptive bond relies on a combination of

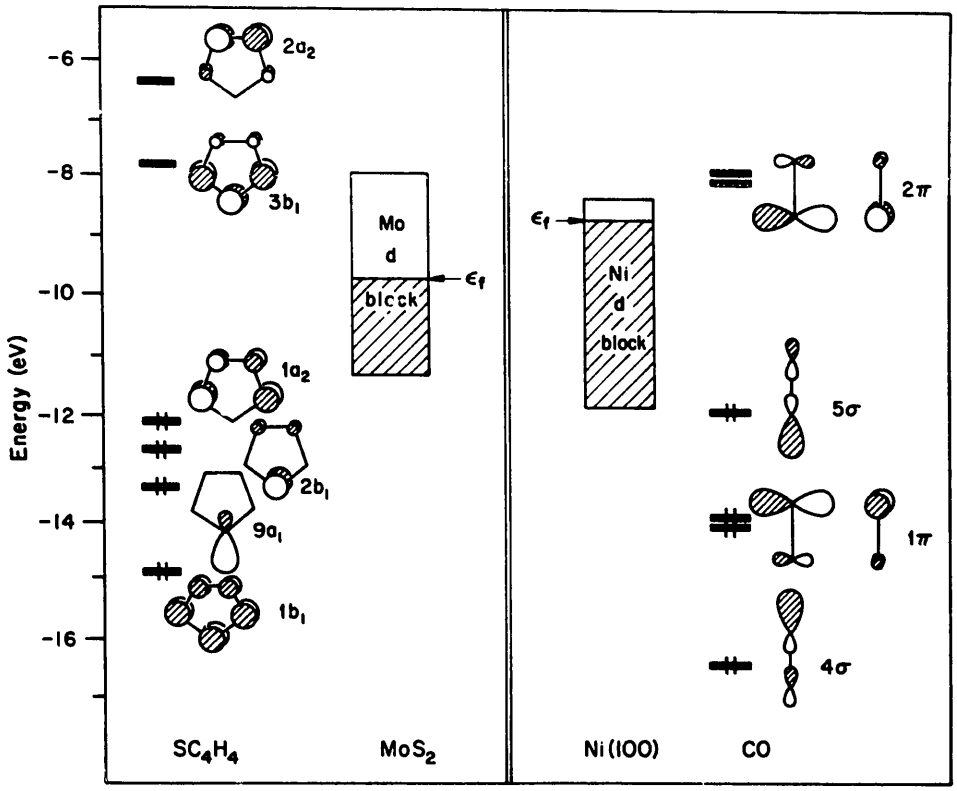

Fig. 2. A schematic comparison of the adsorbate MO's and the metal d blocks in the thiophene/MoS_2 system on the left, and the CO/Ni system on the right.

electron donation from an occupied adsorbate orbital to the surface, and backdonation from the surface into an empty adsorbate level. The prototypical example is the 5σ donation and $2\pi^*$ backdonation of the CO. The same picture can be used for larger, more complex adsorbates such as thiophene. The acceptor orbital of thiophene will be the empty $3b_1$, scheme 9, and the donor orbitals are the two sulfur lone pairs. These are $2b_1$ perpendicular to the ring and $9a_1$ tangential to the ring. The free thiophene levels are shown on the far left of fig. 2, juxtaposed with a block representation of the free Mo d levels (not involved in $Mo-S_{surf}$ bonding). A comparison to the simpler and more familiar levels of the CO on Ni system [32], on the right in fig. 2, can give a rough idea of the donor and acceptor qualities of thiophene. The energy gap between the substrate ϵ_f and the adsorbate LUMO is ~1.8 eV for

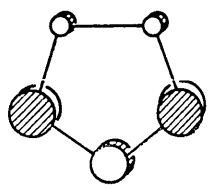

Scheme 9

thiophene/MoS_2 and ~0.5 eV for CO/Ni. The CO $2\pi^*$ is likely to be a better acceptor thiophene $3b_1$. The thiophene sulfur lone pairs lie ~3.0 eV ($2b_1$) and ~3.75 eV ($9a_1$) below the MoS_2 ϵ_f, compared to ~3.0 eV for the CO 5σ. The relative strengths as donors will be determined by the dominating lone pair, which will depend on the coordination site. However, to place this comparison in the proper perspective, recall that CO itself is not a "good" adsorbate on Ni; it does chemisorb, but no dissociation occurs.

4. η^1 and η^5 sites

Initially, let us consider seven possible active site for the thiophene/MoS_2 system. The choices are made on the basis of the transition metal surface studies and the coordination found in organometallic thiophene complexes. The thiophene S–Mo bond distance was set to 1.90 Å in all cases, as this is the minimum distance found in Mo organometallic species [33]. In previous work, we found that the chemisorptive bond length will simply alter the magnitude of the interactions, but will not reverse the general trends or change the nature of the electronic interactions [32a]. Because of the size of the thiophene ring (3.60 Å diameter), the unit cell must contain two primitive substrate cells to prevent interadsorbate interactions. The unit cell thus becomes 6.32 Å long in the translational direction. The ratio of thiophene to surface Mo is 1 : 2.

Of the seven possibilities, the first three place the thiophene S on top of protruding Mo_3. In scheme 10a, the ring is perpendicular to the surface and lies in the *xz* plane. The coordination is η^1. The ring is tilted toward the surface by 45° for scheme 10b (not shown), and in scheme 10c the ring is pushed parallel to the surface. The second three allow the thiophene S to bridge protruding Mo_3 and Mo_6. The ring is again perpendicular to the surface and in the *xz* plane for scheme 10d. It is tilted by 45° for scheme 10e (not shown) and parallel to the surface for scheme 10f. The latter is of particular interest as the ring is nearly centered over Mo_6 in an approximate η^5 coordination. Exact η^5 coordination is not achieved because of the S–Mo bond length restriction. We choose to keep this restriction because both the bond type and bond length must be identical for a valid comparison to be made. The trends in bond strengths we calculate should then be indicative of actual variations in bond lengths. Thiophene is bound to the pristine surface for the last site, scheme 10g. The ring is S bound to a recessed Mo_4. The ring is perpendicular to the surface and lies in the *xz* plane. The tilted and parallel geometries are incompatible with the structure of the lower surface; the thiophene to S_{surf} contacts will be too short. The three perpendicular modes, schemes 10a, 10d, and 10g, were constructed and calculated with the thiophene ring lying in the *yz* plane as well. Negligible differences were observed between the two orientations, thus only the *xz* orientation is discussed.

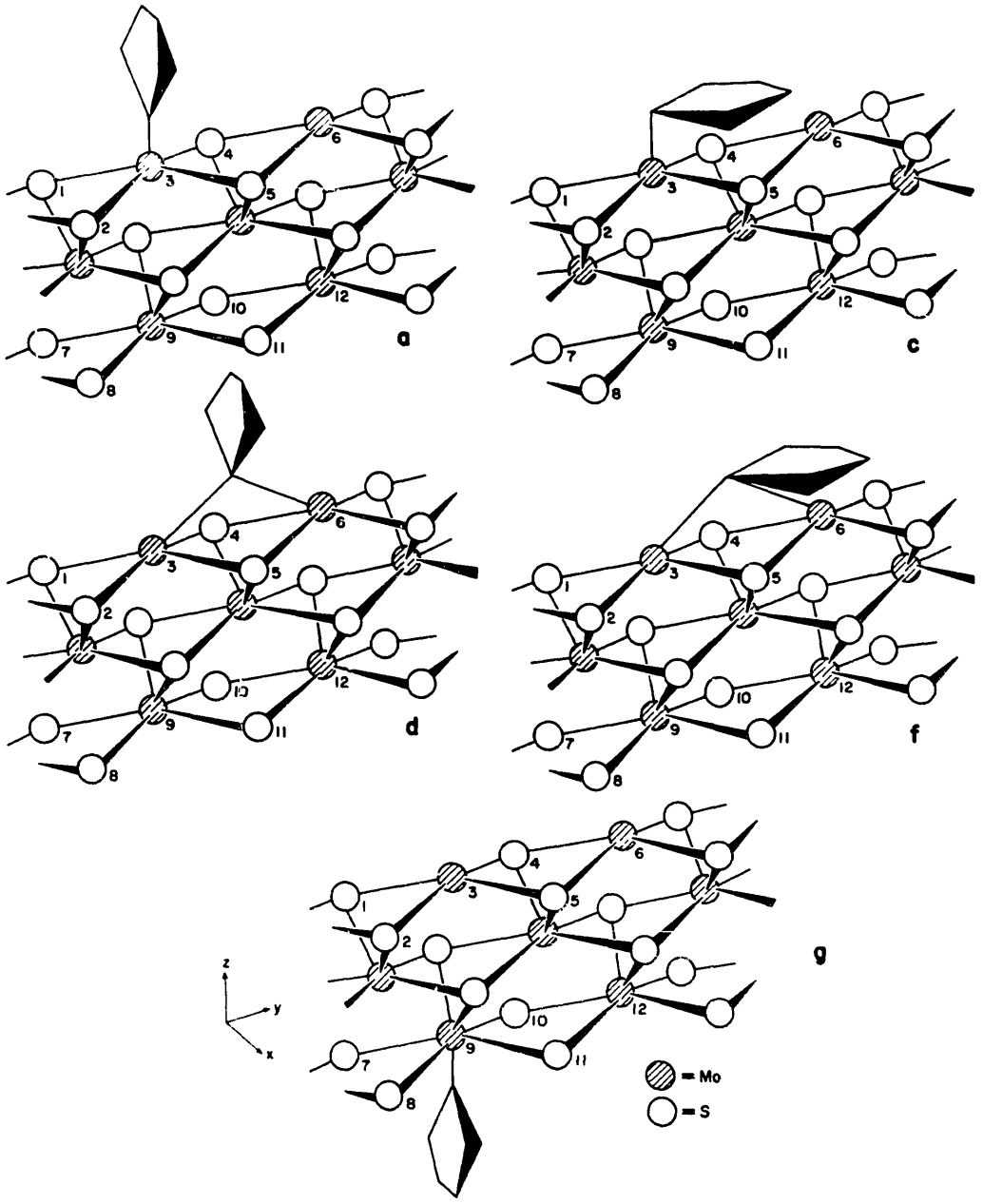

Scheme 10

The crucial thiophene Mo occupations, overlap populations (o.p.) and binding energies (BE) are compiled in table 1. According to the two criteria for the active site – large $3b_1$ occupation and reduced S–C o.p. – the η^5 site, scheme 10f, is the preferred active site. The occupation of $3b_1$ is nearly 3/4 e^- and the S–C o.p. is reduced 12% from the free molecule. To achieve this high activity, it is necessary to have at least two adjacent partially uncoordinated Mo centers, or defect sites. This is simply a matter of geometry; the size of the

Table 1
Thiophene orbital electron occupations

Thiophene MO	On-top			Bridging			Mo_9
	Scheme 10a	Scheme 10b	Scheme 10c	Scheme 10d	Scheme 10e	Scheme 10g	Scheme 10f
$2a_2$	0.000	0.000	0.177	0.016	0.013	0.325	0.045
$3b_1$ (LUMO)	0.014	0.052	0.095	0.028	0.254	0.719	0.168
$1a_2$ (HOMO)	2.000	1.996	1.759	1.968	1.712	1.688	1.990
$2b_1$	1.792	1.803	1.747	1.688	1.571	1.571	1.326
$9a_1$	1.714	1.723	1.788	1.546	1.621	1.842	1.611
Overlap populations							
S–C	0.846	0.836	0.811	0.797	0.808	0.778	0.851
(1.72 Å, 0.887 for free thiophene)							
Mo–S_{thio} (1.90 Å)	1.004	0.947	0.742	0.568	0.725	0.412	0.369
Binding energies (eV) [a]							
	3.20	2.74	1.00	0.85	0.54	−11.97	−11.57

[a] BE = $E(MoS_2$ substrate) + E(free thiophene) − $E(MoS_2$ + thiophene system). Positive BE is attractive, negative is repulsive.

thiophene ring requires at least two adjacent defects for coordination parallel to the surface. Scheme 10f is also, however, the highest energy site. In the sequel, we will focus on adsorption geometries of type of scheme 10f as providing the best activation. So we must deal directly with the extravagently high negative binding energy in this site. Scheme 10f shows so much repulsion between the surface and thiophene because its geometry is highly unrealistic. Fixed Mo–S distances of 1.90 Å in scheme 10f lead to Mo–C_α of 1.5 Å, and Mo–C_β of 1.7 Å. Therefore we move the ring so that the center falls above the Mo, with all Mo–C distances becoming 1.9 Å. The S–C overlap population changes little, to 0.780, still significantly reduced. And the binding energy is a much less repulsive −1.53 eV. The Mo–C distances may still be too short; in $CpMoH_2$ it is 2.3 Å [34]. When we move the ring to that separation the binding energy becomes positive, 1.20 eV. The types of interaction responsible for the high activity of the true η^5 and η^5-like (scheme 10f) modes are identical, but for scheme 10f, they are exaggerated and thus easier to identify and analyze. In summary, while scheme 10f is repulsive, it leads to more favorable bound geometries which also seem prepared for S–C bond cleavage.

The least active site is scheme 10g, bound to the recessed Mo on the pristine surface. S–C bond weakening is negligible and $3b_1$ occupation is 0.17 e^-. It is also a poor choice for the initial adsorption site due to the strong adsorbate–substrate repulsion (BE = −11.57 eV). Because of the full coordination sphere of six substrate sulfur atom, Mo_9 can act neither as donor nor

acceptor. The Mo–S_{thio} (S_{thio} = thiophenic sulfur) interaction is in fact the weakest of the set of seven, with an o.p. of 0.369. The C_α–S_{surf} short contact (2.71 Å) will allow for interaction between $3b_1$ and S p levels. This "through-space" interaction brings ~ 8% of the $3b_1$ levels into the S p block. Each of the four C_α–S_{surf} o.p.'s of −0.08 will contribute to the net adsorbate–substrate repulsion. Clearly, the fully coordinated Mo provides a poor site for catalysis, and the pristine surface must be activated in some manner before catalysis can occur. Our results, as well as experimental evidence suggest that such activation probably occurs through the formation of sulfur vacancies.

At any particular ring orientation (perpendicular, tilted or parallel), the bridging sites are substantially more active than on-top sites, based on $3b_1$ occupation and S–C o.p. reduction. Equivalently, bridging thiophene is a better acceptor, in the Blyholder terminology. It is also a better donor. The total electron loss from the two sulfur lone pairs, $2b_1$ and $9a_1$, is consistently greater for bridging thiophenes. A more reliable measure of the strength of an interaction is the amount of dispersion induced in the projected DOS of the adsorbate MO. As discussed at length in previous work [32a], to consider only the net atomic or MO charge transfer may give erroneous results. For example, a strong interaction can push as many levels below ϵ_f as above. From the charge transfer alone, the interaction will appear weaker than it is. For these seven systems, the dispersion of the sulfur lone pairs of bridging thiophene is greater, verifying that it is the stronger donor. The direction of net charge flow is out of the thiophene to the coordinated Mo, and (except for schemes 10d and 10e) into the uncoordinated surface and bulk Mo's. This suggests that the donor, rather than acceptor, properties of thiophene dominate chemisorption.

Of the two sulfur lone pairs, the more effective donor is the one best able to interact with Mo_{yz}, scheme 8. This can be determined by comparing the dispersions of $2b_1$ and $9a_1$ levels, rather than the charge transfer shown in table 1. Recall that Mo *yz* points out of the surface and is relatively uninvolved in the Mo to S_{surf} bonding. For the on-top sites, the bonding between Mo *yz* and the thiophene MO will be π-type. $2b_1$ will dominate the perpendicular mode, scheme 11a, and $9a_1$ the parallel geometry, scheme 11b. In the case of the bridging thiophenes, the lone pair radial, rather than tangential, to the bridge exhibits the stronger interaction with the Mo *yz*. In organometallic dimers bridged by an isolobal ligand, the role of these two types of orbitals is governed by both the bridging MLM angle (112° in this case) and the relative energetics of the metal and ligand orbitals [35]. $9a_1$ is the radial orbital for the perpendicular coordination, scheme 11c, and $2b_1$ is for the parallel (η^5), scheme 11d.

Now we will consider two systems in detail; scheme 10f since it is the most active site, and scheme 10a exactly because of its low activity, contrary to the evidence of some transition metal surface studies, but in agreement with the

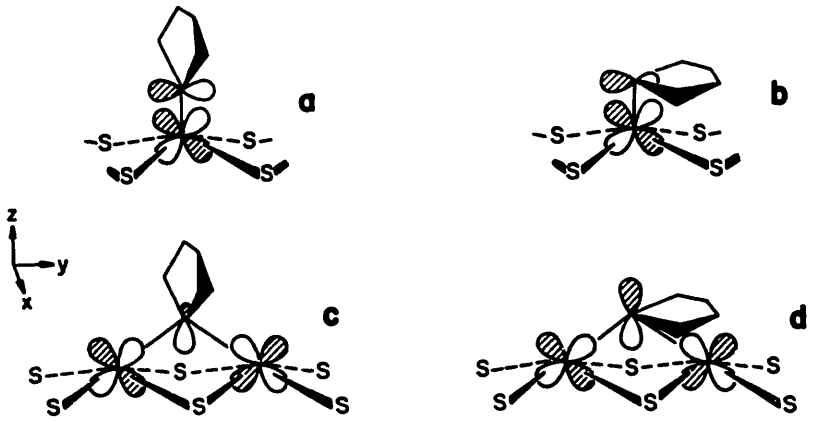

Scheme 11

lack of reactivity of the η^1-thiophene organometallic species. Fig. 3 depicts the total DOS of the η^5 scheme 10f system, and the contributions (magnified) of the thiophene $3b_1$ and metal $x^2 - y^2$ orbitals to the DOS. Interacting orbitals are identified by resonances in the density of states contribution. The process is similar to finding mixing in molecular systems by analyzing the orbital coefficients. That could be done in the crystal orbitals as well, but because the coefficients at so many points in the Brillouin zone would have to be considered, it is easier to move to the DOS curves and find interactions by matching peaks in these curves. Note that one could also spot these resonances

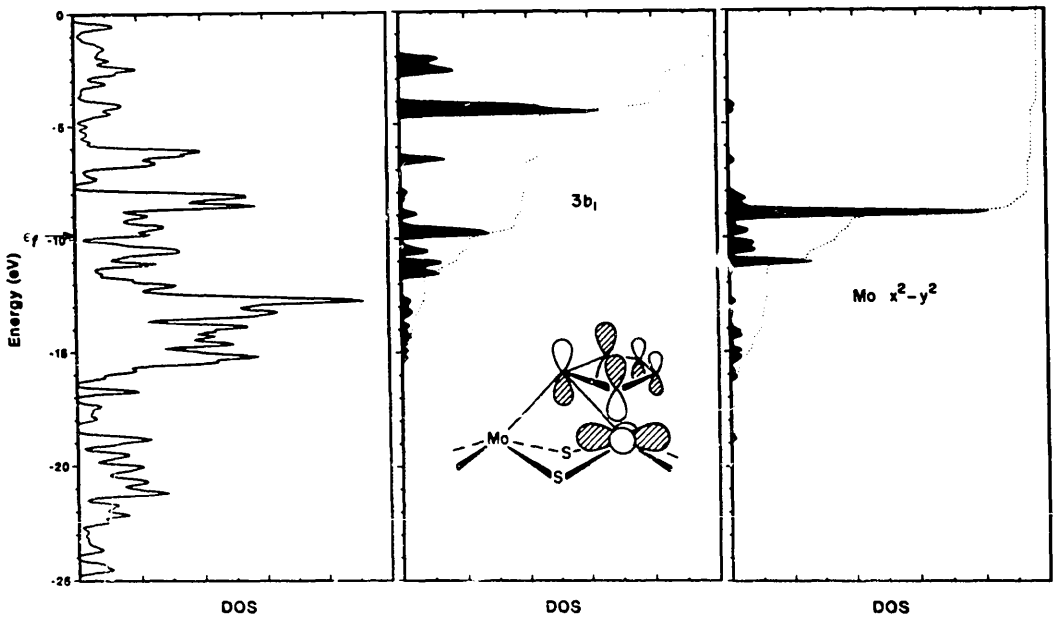

Fig. 3. The total DOS of the η^5-thiophene/MoS_2 system in the left panel, the magnified projections (15×) and integrations of the $3b_1$ and Mo $x^2 - y^2$ in the middle and right panels, respectively.

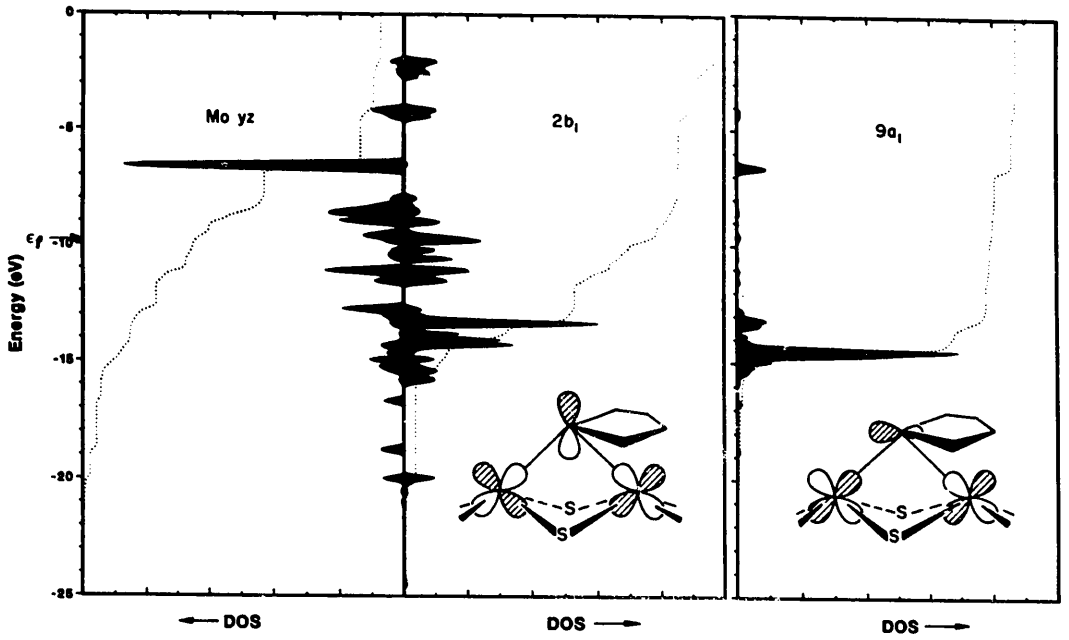

Fig. 4. Projected DOS and integrations of the η^5-thiophene/MoS_2 system: Mo *yz* in the left panel, thiophene $2b_1$ in the middle, and $9a_1$ on the right.

by just looking at the integration curves, and this we will do for the remainder of our study. In this case, the match between $3b_1$ and Mo x^2-y^2 is good, and dispersion of $3b_1$ caused by the interaction is very large. The molecular energy value is -7.87 eV, but $\sim 30\%$ of the levels are found in the Mo d block and $\sim 10\%$ pulled as far down as the S p block.

In fig. 4 are depicted the projected DOS and integrals of $2b_1$, Mo *yz* and $9a_1$ in the left, middle and right panels respectively. Compare the dispersion of the lone pairs, and indeed the radial $2b_1$ is greater. The match in the peak positions of $2b_1$ and Mo *yz* is also stronger. On bare MoS_2, these surface levels fill the semiconductor gap (fig. 1), but are now spread over a wide energy range. $9a_1$ is not entirely unaffected by adsorption. The bulk of the levels is pushed only ~ 1 eV below the -13.32 eV molecular level, but $\sim 12\%$ are driven up above the energy window. The resonance is particularly strong at -6.5 eV.

Several η^1-thiophene bonding modes have been identified on transition metal surfaces and in organometallic complexes. Our calculations show the η^1 scheme 10a system to be only a fair active site for S–C weakening, but the most favorable site energetically. The 3b occupation is 0.01 e^-, the S–C o.p. reduction is 4.5%, but the binding energy is $+3.2$ eV. That η^1-coordinated Mo is a good adsorption site, but a poor active site is simply because Mo is a better acceptor than donor. On the left in fig. 5 are the thiophene $3b_1$ and $2b_1$ and Mo *yz* integrations. The bars on the right axis identify the $3b_1$ and $2b_1$ free thiophene energies. Both thiophene orbitals mix with the Mo *yz*, as would

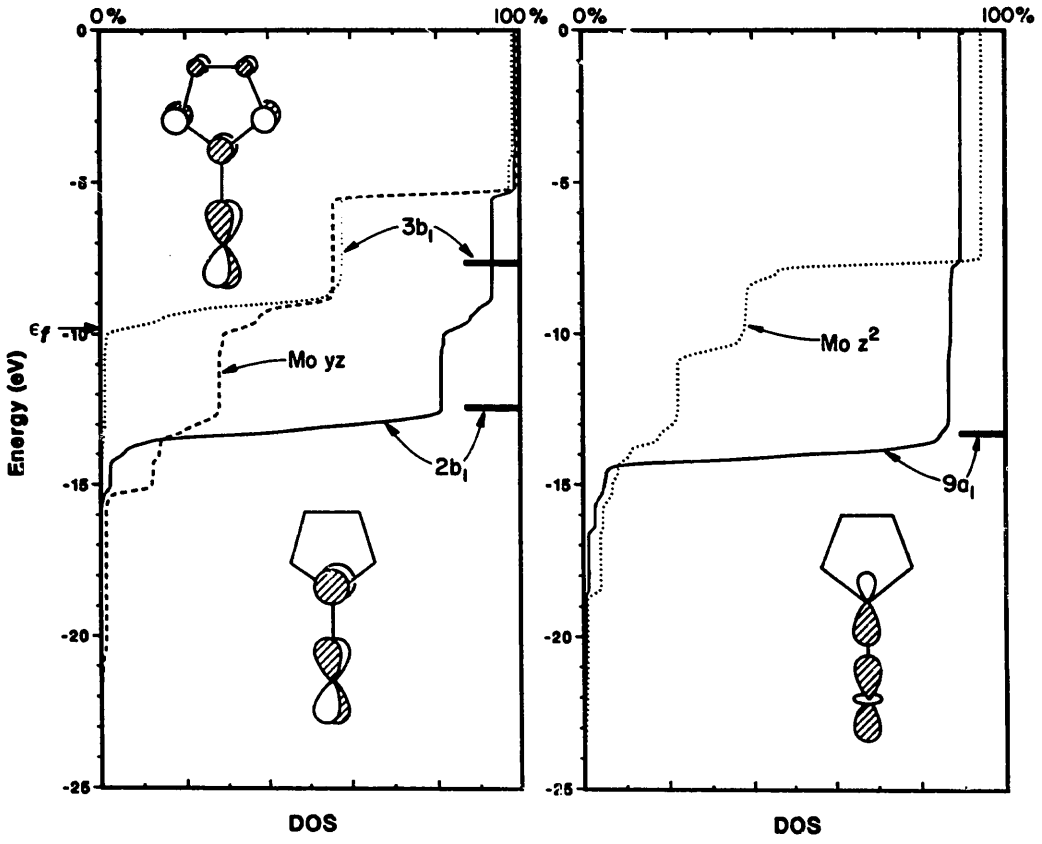

Fig. 5. The η^1-thiophene/MoS_2 system: the integrals of $2b_1$ (solid line), Mo *yz* (dashed line) and $3b_1$ (dotted line) in the left panel, and those of $9a_1$ (solid line) and Mo z^2 (dotted line) in the right panel.

be predicted from the orbital symmetries. Three distinct peaks emerge from the three level interaction; the lower predominantly $2b_1$, the middle, near ϵ_f, original Mo *yz*, and the upper, $3b_1$. On the bare surface, *yz* occupation is 1.14 e^-, but the $2b_1$–*yz* interaction is so strong that a large number of the *yz* levels are pushed above ϵ_f, resulting in a loss of 0.46 e^-. Because the Fermi energy is essentially constant (and ideally should remain fixed) the electrons lost by thiophene will be dumped into other substrate levels, which are the adjacent surface and bulk Mo in the η^1 case. The $3b_1$–Mo *yz* coupling strength can be gauged by the appearance of ~ 45% of the $3b_1$ levels in the middle (*yz*) peak. Few of the $3b_1$ levels fall below ϵ_f because the Mo *yz* band has been pushed up so strongly by the better overlap with the S localized $2b_1$.

In the right panel of fig. 5 are the $9a_1$ and Mo z^2 integrations. The interaction is strong; the $9a_1$ median energy (energy of half filling) falls ~ 1 eV below the free thiophene level and its electron loss is comparable to that of $2b_1$ (-0.29 e^- for $9a_1$ and -0.21 e^- for $2b_1$). In addition, the upward shift of z^2 causes a 0.33 e^- loss relative to the bare surface. A multi-level interaction is again at work. Both Mo s and p_z are of the proper symmetry to mix with z^2

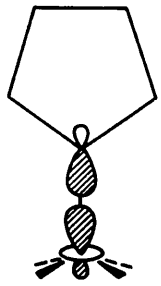

Scheme 12

and create a hybrid orbital pointing out of the surface and well localized for $9a_1$ bonding, scheme 12. Since such orbital mixing is often simpler to analyze in molecular systems, we construct the hypothetical molecular analogue of the coordination site, $MoS_4(SC_4H_4)^{-4}$ [36]. Analysis of the molecular orbitals of this model show that the formally z^2 MO is in fact derived ~ 30% from p_z; the s component is small due to the large energy gap. This confirms the picture in scheme 12.

Returning to the left panel of fig. 5, the η^1 mode can perhaps become a more active site if the surface is somehow reduced. The $3b_1$ levels directly above ϵ_f would then become occupied. Reduction may come about at a lower coordinated Mo center (a more "defective" site) or on a binary metal sulfide surface [30,37]. Both possibilities will be discussed.

5. η^2 coordination

One intriguing possibility of raising the ring-to-surface contact is an η^2-thiophene coordination, such as in scheme 13. This geometry has been suggested as for the intermediate in a two-step mechanism of sulfur extrusion [20]. Many geometric options are conceivable, from the simple scheme 13 to complex bridging constructions. But few choices will avoid a very strained and awkward four-coordination planar arrangement about C_α; dehydrogenation may need to occur first. Dehydrogenation products are observed on the clean

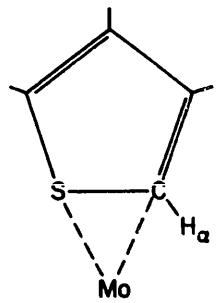

Scheme 13

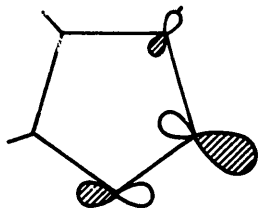

Scheme 14

transition metal surfaces under low H_2 pressure. As model studies on MoS_2, as well as the actual industrial catalysis process, are conducted under hydrogen atmospheres, it is not surprising that such products are not found. However, a reasonable HDS mechanism might well incorporate a partial dehydrogenation step immediately preceding desulfurization, and then conclude with full hydrogenation. For example, H_α could be temporarily lost or hydrogen bridged to a surface sulfur, and regained after desulfurization. Precedence for the formation of a S–H surface species can be found in the inelastic neutron scattering measurements on H_2 sorption onto MoS_2 [38a] and the observation of S–H stretching frequencies by IR [38b,38c]. We cannot follow the dehydrogenation process directly, since the potential energy surface we would generate for such a complex scenario would be unreliable. We can consider one potential waypoint – the α-dehydrogenated $SC_4H_3^-$ adsorbate. The $SC_4H_3^-$ molecular levels naturally closely resemble the thiophene orbitals. The localization of $2b_1$ and $9a_1$ is not as strongly on the sulfur. A $3b_1$-like orbital is the LUMO, and remains at approximately the same energy. The important difference is the emergence of a new HOMO, scheme 14. It is essentially a C_α lone pair; the destabilized remains of the C_α–H bond. It is somewhat S–C σ bonding, thus allowing a new avenue for S–C bond weakening by possible depopulation of that orbital. The S–C o.p. is 0.882, nearly the same as thiophene.

We consider two η^2 modes bound to a single Mo: scheme 15a, ring in *xz* and perpendicular to the sandwich propagation direction, and scheme 15b, ring in *yz* and "along" the sandwich. The two bridging modes are scheme 15c, ring in *xz*, and scheme 15d, ring in *yz*. The S–Mo and C–Mo bond lengths are set to 1.90 Å. A summary of the results is given in table 2. S–C bond weakening is most vigorous in scheme 15c (~ 25% reduction), although the binding energy is unfavorable. Scheme 15b may be the best compromise; the adsorbate–substrate interaction is attractive, and the S–C o.p. reduction is comparable to the η^5 system.

The mechanism for S–C bond scission is apparently very different for η^1- or η^5-thiophene than for η^2-$SC_4H_3^-$. For η^1- or η^5-thiophene, the extent to which $3b_1$ can act as an acceptor determines the amount of bond weakening in thiophene. The donor characteristics of the adsorbate are important in the

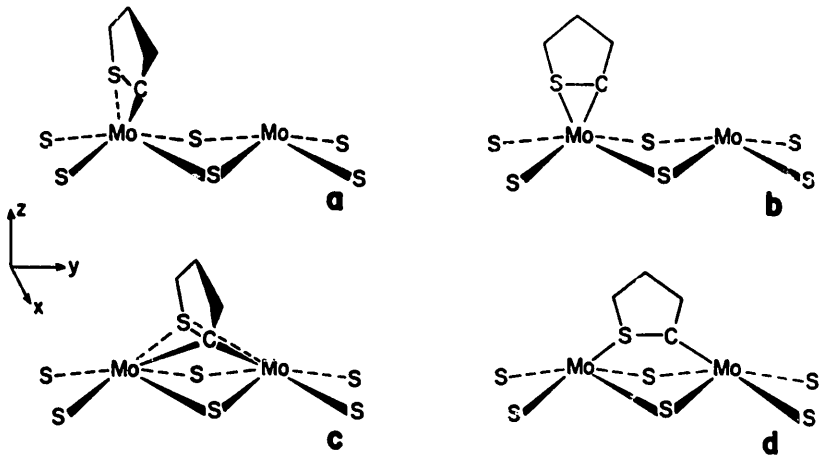

Scheme 15

chemisorptive bond formation, but not to the S–C scission. The η^2-$SC_4H_3^-$ orbital occupations reveal a different scenario. The acceptor capacity of the unoccupied levels is essentially lost; the occupation of the "$3b_1$" orbital is never more than 0.074 e^-. But the HOMO, the C_α lone pair, acting as a donor takes over the role played by the $3b_1$ in thiophene desulfurization. Recall that the orbital is somewhat S–C_α bonding, thus removal of electrons from the level will weaken the bond. It is a good donor; better than the combined two sulfur lone pairs based on the electron losses. The C_α lone pair depopulation runs parallel to the S–C o.p. trends, and no such correlation can be found with the $3b_1$ electron gains. Roughly speaking, the S–C bond is weakened in favor of the new C–Mo chemisorptive bond. Although we have a good estimate of the former effect in the S–C o.p., the later is difficult to gauge. The diversity in coordination number and mode cannot easily be accounted for in the Mo–S and Mo–C o.p.'s.

The sites of schemes 15a and 15b are geometrically so similar, that they can be compared side by side. If the thiophene lies "along" the sandwich, in *yz* as in scheme 15b, the S–C weakening is considerably more than "across" the sandwich, in *xz* as in scheme 15a. The resonances are strong between both the C_α lone pair and *yz* of scheme 15b, *xz* of scheme 15a. The electron loss from

Table 2
η^2-thiophene results

	Scheme 15a	Scheme 15b	Scheme 15c	Scheme 15d
$3b_1$ occupation	0.035	0.039	0.074	0.614
C_α lone pair	1.460	1.335	0.900	1.508
S–C overlap population (0.887 for free thiophene)	0.844	0.784	0.669	0.818
BE (eV)	3.38	2.23	−4.14	5.88

the adsorbate orbital is greater for scheme 15b. The answer can lie in the additional interaction possible only in scheme 15b between the adsorbate and the adjacent bare surface Mo. The distance is long (2.86 Å) and the overlap population small (0.064), but the contact can induce important rehybridization in the adsorbate levels.

6. Ring hydrogenation

Direct hydrogenation of the thiophene ring is frequency proposed as a critical step toward S–C scission, particularly in the context of hydridic addition to η^5-organometallic complexes [23]. It has been suggested that the loss in conjugation afforded by the addition reaction could overcome a potential barrier in HDS [39]. Hydride addition is specific to the α position for the organometallic compounds [23]. Under catalytic conditions, however, it is unclear whether the addition will be of H^+, $H^\cdot$, or H^-. Heterolytic H_2 cleavage may be favored over homolytic cleavage on MoS_2 [26].

The large α-carbon coefficients of both the $3b_1$ LUMO and the $1a_2$ HOMO (fig. 2) favor α over β hydrogenation by H^+, $H^\cdot$, or H^-. But as previously mentioned, $2b_1$ is part of the π system and is not a "pure" lone pair. The density is ~ 29% at each β-carbon. Thus β-H^+ addition appears possible, but β-$H^\cdot$ or H^- addition will be hampered by the low orbital density of $3b_1$ at β-C.

The interaction diagrams of α and β hydrogen addition to an isolated thiophene molecule, not bound to a MoS_2 surface, are shown respectively on the left and right in fig. 6. The approach is in a perpendicular direction, d(C–H) = 1.0 Å, Orbital occupations are given for the case of H^+. The extent of stabilization of $1a_2$ due to α-addition and $2b_1$ for β-addition are very similar, as is the stabilization of the all π bonding $1b_1$. The α-H^+ product is energetically favored by only 0.10 eV. What is more intriguing is a comparison of the ring o.p.'s, scheme 16. Both addition geometries weaken one and strengthen the other S–C bond, but the weakening upon α-addition is much more profound. The interaction diagrams show that symmetry reduction by the incoming hydrogen allows a strong mixing of $3b_1$ into the $1a_2$ level. The resultant orbital, 3α, has significant S–C antibonding character. Mixing resulting from the β-addition does not create an occupied orbital so strongly S–C antibonding.

Addition of either $H^\cdot$ or H^- will partially or fully populate the $3b_1$ derived level. Because of the larger α coefficients, the stabilization of this orbital from an α approach is greater. The total energies favor α over β by 0.44 eV for $H^\cdot$ and 0.97 eV for H^-. α-addition remains ~ 9% more effective towards S–C weakening for $H^\cdot$, but for H^-, it is β-addition which results in a weaker S–C bond.

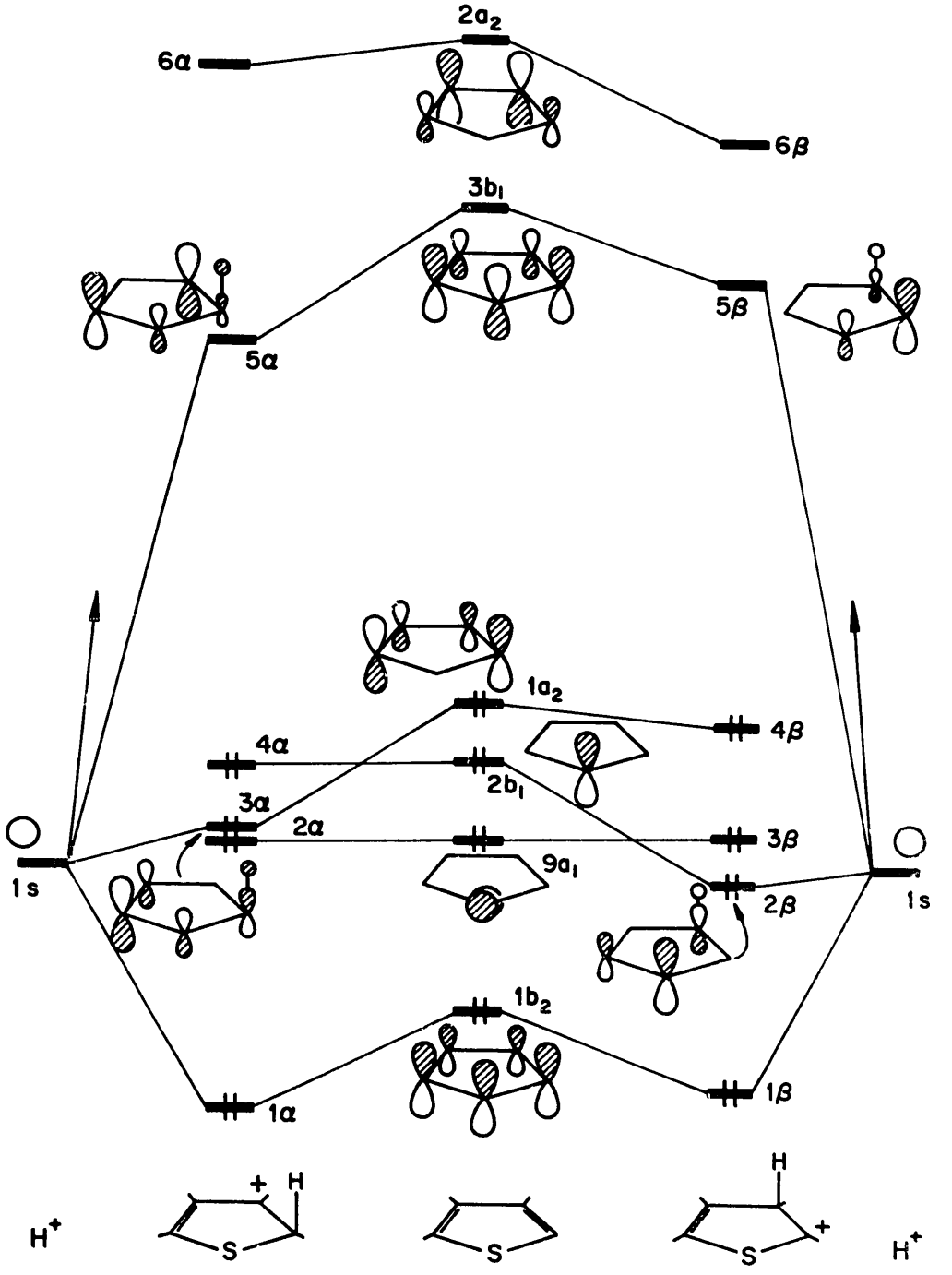

Fig. 6. Interaction diagram of α-hydrogenation of thiophene on the left, and β-hydrogenation on the right.

Similar trends result if hydrogen addition occurs onto thiophene now coordinated η^1 or η^5 to the MoS_2 model, scheme 6. α-H^+ addition is energetically favored over β-addition to both η^1 (0.39 eV/unit cell) and η^5

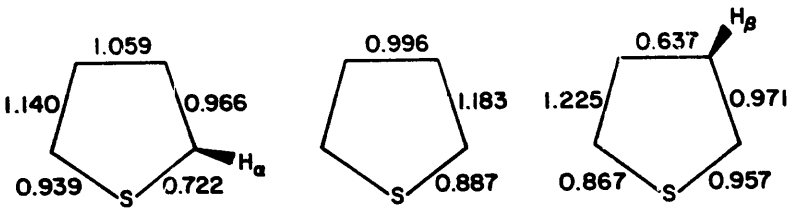

Scheme 16

(0.18 eV/unit cell) adsorbed thiophene. The effect of the hydrogenation step alone on the S–C o.p. also parallels the molecular results. In each case, one S–C bond is weakened while the other is strengthened in comparison to the results of thiophene bound to the surface, schemes 10a and 10f. The reductions are 13–14% in the o.p.'s for the α-products, but only 1–2% for the β-products. All in all, it appears that α-addition is not only somewhat favored over β-addition, but it may also help to activate the ring toward a two-step desulfurization process in which the two S–C bonds will be broken independently.

7. Other defect sites

A fundamental problem in establishing an HDS mechanism is the lack of information about the surface morphology of the catalyst at an atomic level. Thus far, we have considered thiophene adsorption onto the pristine MoS_2 edge plane (bottom plane of scheme 6) and onto simple two vacancy defect sites created by removing a plane of sulfur atoms (top plane of scheme 6). A more explicit defect site can be produced by sequentially removing one to three of the four S_{surf} atoms about each protruding Mo. The removal of one S_{surf} from this plane will create a three vacancy site. Such sites have has been examined as models for the potentially active corner of the MoS_2 crystal [24c]. Further S_{surf} removal will perhaps unrealistically deform the MoS_2 structure, as these sulfurs are coordinated to bulk Mo as well. The results can, however, be directly compared to calculations on schemes 10a–10f, so that the direct effect of the defect on the binding mode can be examined. The sulfurs are removed as neutral atoms, so that the Mo is formally reduced from Mo (IV) of bulk MoS_2 towards Mo(III). Recall that our calculations start with the protruding surface metals of scheme 6 reduced relative to the bulk. These metals gain approximately an additional 0.4 e^- with each sulfur removed.

As the sulfurs are removed from the top place of the model, the activity of the η^1 site remains constant. The S–C o.p. drops insignificantly from 0.846 in scheme 10a to a minimum of 0.842 if two S_{surf} are removed. The rise in the $3b_1$ population is similarly small (0.005 e^-), and the BE becomes more favorable by 0.31 eV. A defect created by simple coordinative unsaturation of the

Table 3
η^5-thiophene orbital electron occupat ons upon removal of surface S from top surface of scheme 10f

Thiophene MO	Scheme 10f	Remove S_4 [a]	Remove S_4 and S_5	Remove S_4, S_5 and S_1
$2a_1$	0.325	0.372	0.462	0.478
$3b_1$ (LUMO)	0.719	0.720	0.729	0.751
$1a_1$ (HOMO)	1.688	1.719	1.764	1.828
$2b_1$	1.571	1.574	1.582	1.674
$9a_1$	1.842	1.614	1.621	1.621
Overlap populations				
S–C (0.887 in free thiophene)	0.778	0.762	0.758	0.715
$Mo–S_{thio}$	0.412	0.885	0.981	0.990
Binding energies (eV)				
	−11.97	−7.00	−2.48	+1.87

[a] Numbering refers to scheme 10f.

surface will not force the occupation of the $3b_1$ peak directly above ϵ_f in fig. 5. It is of course possible that η^1 coordination at some other defect site may still reverse the low activity of this adsorption geometry.

The effect on the η^5 geometry is striking. Table 3 enumerates the results through the series as 0 to 3 S_{surf} atoms are removed. Thiophene becomes a better backbonder as seen in the dramatic rise of the $3b_1$ occupation (0.719 e^- to 0.751 e^-). The S–C bond weakens as a result, with a drop in the o.p. from 0.778 to 0.715. The BE increases steadily so that the substrate–adsorbate interaction becomes attractive at the removal of the third S_{surf} atom. This type of defect will offer a superior site to a thiophene coordination which is already "activated", as the η^5 mode is.

To understand the effect, we turn to a simple molecular model, the CpMo fragment. The interaction diagram between the orbitals of the $C_5H_5^-$ cyclopentadienyl anion and the Mo d block are shown in fig. 7. The Cp e_2 set, from which are derived the nondegenerate thiophene $3b_1$ and $2a_1$, can interact with the Mo e_2, the xy and x^2-y^2. In the top surface of scheme 6, the xy orbitals are fully occupied with $Mo–S_{surf}$ bonding. But as the S_{surf} atoms are removed, the interaction between the unoccupied thiophene levels and the Mo xy is "turned on", as it is fully for CpMo. More of the $3b_1$ levels will be pulled under ϵ_f. The xy projected DOS corroborate these notions; of the 30% of the xy levels found in the S p block for scheme 6, but less than 10% remain if three S_{surf} atoms are pulled out.

If instead, S_{surf} atoms are removed from the pristine surface, i.e. the bottom face of scheme 6, one, two and three vacancy sites will result. Because of the trigonal prismatic Mo coordination, the two vacancy site will not be identical

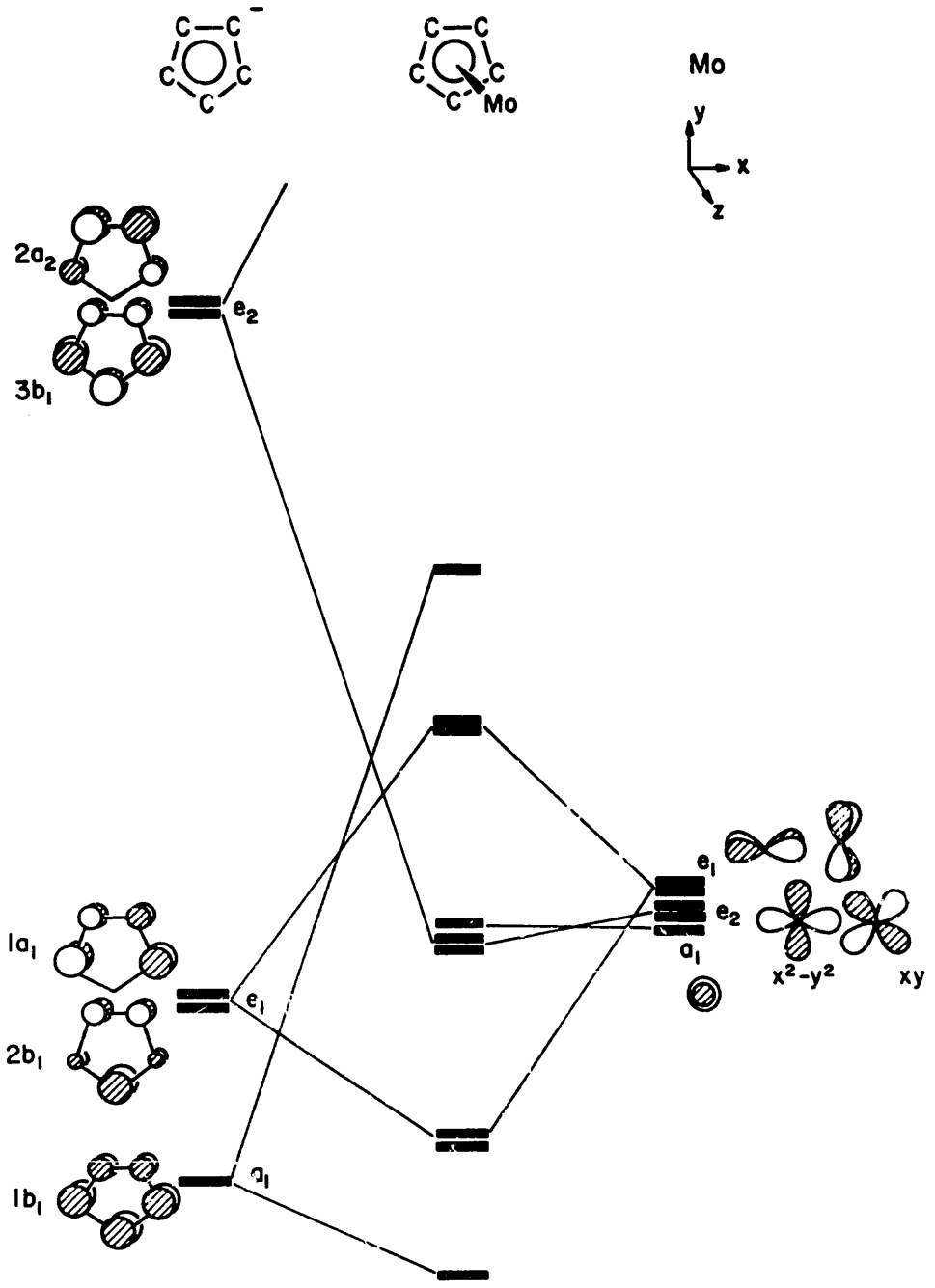

Fig. 7. Partial interaction diagram of the cyclopentadienyl anion on the left and the atomic orbitals of Mo on the right.

to Mo_3 and Mo_6 in scheme 6. Reduction at the metal follows S abstraction on this surface as well; removal of one, two and three S_{surf} atoms produces a gain of 0.19, 0.73 and 1.17 e^- respectively. Nethertheless, S–C activation does not follow in the η^1 scheme 10g system as the surrounding sulfurs are removed. In

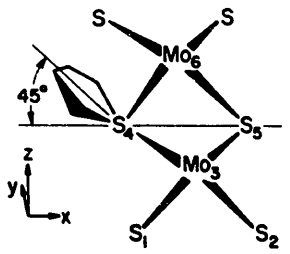

Scheme 17

fact, the S–C o.p. rises nearly imperceptibly from 0.851 on the pristine surface to 0.853 at the three vacancy site. The defect site is a better initial adsorption site; the BE becomes more attractive by ~ 10.6 eV through the series. This could have been predicted, recalling the two factors – low Mo–S_{thio} o.p. and negative C_α–S_{surf} o.p. – which made the site unfavorable on the pristine surface. As S_{surf} atoms are removed, the negative C_α–S_{surf} interaction becomes irrelevant, and the Mo d levels are freed from Mo–S_{surf} bonding and available for Mo–S_{thio} bonding. The Mo–S_{thio} o.p. more than doubles between the pristine and three vacancy site (0.369 to 0.858). The loss of C_α–S_{surf} coupling will lower the $3b_1$ occupation, whereas the heightened Mo–S_{thio} bonding will raise it. The net result is a slight gain in population – from 0.168 e^- to 0.184 e^-.

New thiophene adsorption modes are exposed in the process of creating coordinatively unsaturated defects. For example, one could imagine assigning the thiophenic sulfur to a site previously occupied by a S_{surf} atom. We have chosen a geometry in which the thiophene ring makes an angle of 45° with the edge plane, scheme 17. Numerical results of the series are found in table 4. Simple substitution of S_{thio} for a single S_{surf} atom sets the Mo–S distance at 2.36 Å, which is apparently too long to have any activating characteristics. The $3b_1$ occupation is nearly zero, and the S–C o.p. is invariant from the molecular value. The activity is greatly increased if the Mo–S_{thio} distance is shortened to 1.90 Å by sliding S_{thio} up the Mo–S_{surf}–Mo plane. The $3b_1$ occupation jumps to nearly 1/3 electrons, and the S–C o.p. drops by 0.033. The BE, however, is

Table 4
Substitution of thiophene for surface sulfur

	Remove S_4 Mo–S_{thio} distance		Remove S_1, S_2 and S_4 Mo–S_{thio} distance	
	2.36 Å	1.90 Å	2.36 Å	1.90 Å
$3b_1$ occupation	0.067	0.295	0.048	0.246
S–C overlap population (0.887 in free thiophene)	0.888	0.855	0.873	0.839
BE (eV)	−10.54	−15.30	−0.06	−2.59

strongly repulsive. The site become energetically more tractable if two S_{surf} atoms are removed in addition to the one at the substitution site. The S–C o.p. drops again to 0.839 revealing an increase in activation as well. It is then possible to activate the thiophene ring toward S–C bond weakening through coordination at the sulfur. Of the sites we have chosen to study, however, this activation occurs only when the ring sulfur substitutes for a MoS_2 sulfur. This suggests a multitude of additional sites for future study.

The evidence that defect sites can elevate HDS turnover rates is strong. It is not know, however, whether surface reconstruction occurs on the active surface, because LEED studies have yet to be performed on the edge face. The method has been implemented on the basal plane [4]. A simple type of reconstruction is a pairwise distortion. Similar reconstruction patterns are widely accepted to occur on other semiconductor surfaces (e.g. Si(001)2 × 1 [40]). The idea of S–S dimers is also reminiscent of the non-layered dichalcogenides, that is, the marcasite and pyrite structures of the late transition metals and the pairing that one observes in metal trichalcogenides, such as $NbSe_3$. It has also been suggested that formation of S–S dimers may play a role in HDS catalysis [2a]. We have considered only S–S or Mo–Mo pairing by contraction of the contact distance. Certainly, more complex possibilities could be imagined. On the protruding surface in particular, one might envisage systems which combine the creation of additional defects with S–S pairing. The sulfur pairs can be created across the sandwich along x, scheme 18a, or either symmetrically, scheme 18b, or unsymmetrically, scheme 18c, along y. Both symmetric pairing along x, scheme 18d, and along y, scheme

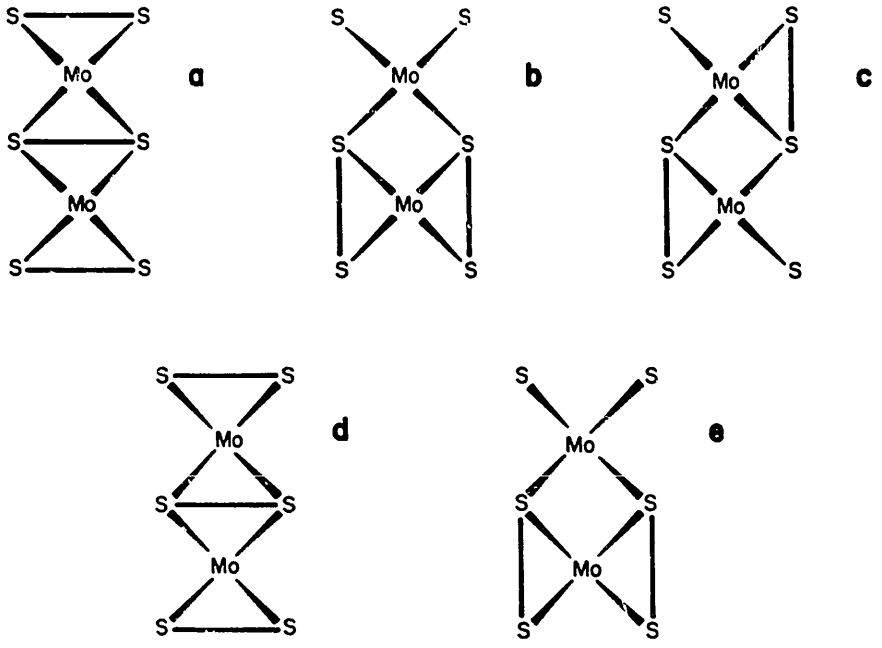

Scheme 18

18e, was considered on the face where Mo is recessed. The latter are of particular interest since they are truly edge sulfurs. The S–S distances in bulk MoS_2 are 3.16 Å along y and 2.98 Å along x. For scheme 18a, contractions less than 0.2 Å were slightly stabilizing (0.13 eV at 0.15 Å), but further contraction of scheme 18a or any contraction whatsoever on schemes 18b–18e were destabilizing. The repulsive S–S behavior can be predicted simply from the total DOS of the original surface (fig. 1). As ~ 80% of the S p levels lie below ϵ_f, dimerization will push partially occupied S–S antibonding levels up in energy. The S–S o.p. will become more negative as a result. A point is reached during the contraction (between d(S–S) = 2.5 and 2.6 Å along y) where the σ^* levels are pushed above ϵ_f and the S–S o.p. rises dramatically. The distortion causes other antibonding interactions to appear and forces the ϵ_f up; the net result remains energetically unfavorable. Based on these results, no simple S–S dimerization is expected.

Mo pairing on both the protruding and recessed surfaces has been examined. The latter is energetically unfavorable at any contraction distance, presumably since the coordination sphere of the recessed Mo is already full. Of the seven reconstruction possibilities we have considered, only dimerization of the protruding Mo is found to be favorable. The total energy per unit cell (108 valence electrons) is reduced by 0.1 eV upon a 0.45 Å contraction to d(Mo–Mo) = 2.71 Å. As the contact is shortened, more of the bonding xz combinations drop below ϵ_f. The yz occupation rises from 0.30 to 0.81 e^-, and the Mo–Mo o.p. doubles with the same contraction. Because the surface bonds become so strong, we expect that the reconstruction will not create strong HDS active sites. Empirically, according to the principle of Sabatier, it seems that good catalysts must have an intermediate heat of formation, i.e. intermediate surface bond strengths [41]. Testing several thiophene adsorption geometries, we find that the reconstruction has no effect on the S–C o.p. of the η^1 species. The η^5 site becomes less active; a 0.45 Å contraction causes the S–C o.p. to increase from 0.778 to 0.805 and the backbonding into $3b_1$ to drop from 0.719 e^- to 0.562 e^-. This is a direct consequence of the heightened Mo–Mo interaction forced by the pairing. Recall that the strongest $3b_1$–Mo mixing is seen with $x^2 - y^2$. The combinations which are σ bonding between the metals, exactly those which can interact with $3b_1$, will move to a lower energy and further from the thiophene level. Nethertheless, the site retains a greater activity than the remaining six geometries on the unreconstructed surface (scheme 10).

8. Promotion and poisoning

It is well known that MoS_2 (or WS_2) treated with cobalt or nickel will exhibit enhanced HDS activity. Turnover rates can be increased by as much as

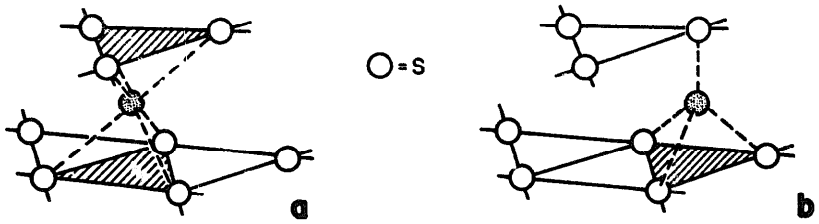

Scheme 19

a factor of ten [42]. The effect is synergistic, as the activities of the promoted systems are greater than either sulfide individually. A recent study has also shown that copper can act as a very efficient poison and reduce MoS_2 activity by ~ 50% [37]. The mechanism of promotion or poisoning is still an unresolved issue. The promoter atoms are likely to remain near or at the crystal surface, in what has been described as a "decoration" process. Among the various models following this hypotheses, there is strong support for the "pseudointercalation" model. The idea is that Co and Ni insert into the edge face between the S–S layers to occupy the octahedral and/or tetrahedral holes near the surface. These sites are shown in schemes 19a and 19b, respectively. The pseudointercalated promoter will work indirectly on existing surface sites to enhance their activity. The term "pseudointercalation" was originally applied to the WS_2/Ni hydrogenation catalyst [43] and later to the MoS_2/Co HDS system [44]. It serves to emphasize that normally, neither MoS_2 nor WS_2 are subject to ready intercalation, in contrast to other layered dichalcogenides. A recent Auger spectroscopy study of the Co/MoS_2 system found Co absent from the basal plane. The depth profiles obtained by sputtering away the edge plane reveal substantial Co enrichment near the crystal surface, dropping from ~ 23% at the surface to ~ 12% at 160 Å, and trace amounts at 1500 Å [45]. Mössbauer emission results indicate that the Co resides in a sulfur environment [42,46]. However, the authors propose a second type of "decoration"; Co can substitute for Mo near the crystal surface [46]. The promoter can assume a direct role in the reaction, providing a new type of site rather than modifying the existing Mo sites.

Proponents of a third model, the biphasic or contact synergy model [47], contend that promotion results simply from the direct contact between MoS_2 (or WS_2) and Co_9S_8 (or Ni_3S_2) crystallites. The evidence consists primarily of the lack of contamination in the MoS_2 phase as analyzed by micrography [48]. Although a second phase is often detected, the previously referenced Mössbauer studies can be used to argue against its direct role in promotion and catalysis. A number of other models have also been advanced in the past for the synergist effect of Co and Ni [49], their disparity stemming perhaps from the difficulty and variability of sample preparation.

Apart from the geometric considerations, there is also the difficult question as to whether the modification is in the quality of the active site (electronic effect) or in their quantity (structural effect). The electronic mechanism is favored both by modeling studies of HDS activities [9] and the observation of a relationship between the turnover rates of the synergistic systems and the average of the component sulfide heats of formation [50]. The nature of the electronic effect has been addressed through a series of SCF-Xα calculations on $MoM'S_9^{n-}$, M' = V to Zn [30,37]. It was found that because of the relative energy of the d orbitals, Co and Ni transfer electrons to Mo, whereas Cu acts as an electron withdrawer. These results were consistent with the previous calculations on binary metal sulfides which related electronic factors to trends in HDS activity [25]. It was suggested that in the Co or Ni promoted systems, the increased d electron density on Mo would strengthen the metal–thiophene interaction and increase backbonding into the thiophene ring.

In order to investigate both the geometric models and the electronic factors at work in the bimetallic systems, we construct a series of models testing each of the three metals – Co, Ni and Cu – at each of three sites – substituted, octahedral and tetrahedral. The second atom can simply be substituted for a molybdenum atom in the one-dimensional model; our choice is Mo_6 in scheme 6. The ratio of protruding Mo to substitute metal is 1 : 1. Both octahedral and tetrahedral sites are available for pseudointercalation between the S–S layers, schemes 19a and 19b. The single sandwich of model 6 is clearly an inadequate unit cell. Two of the three layers of two adjacent unit cells are depicted in scheme 20. To create the correct S–S registry, this new unit cell must contain sections from two adjacent sandwiches and must be translated in both the x

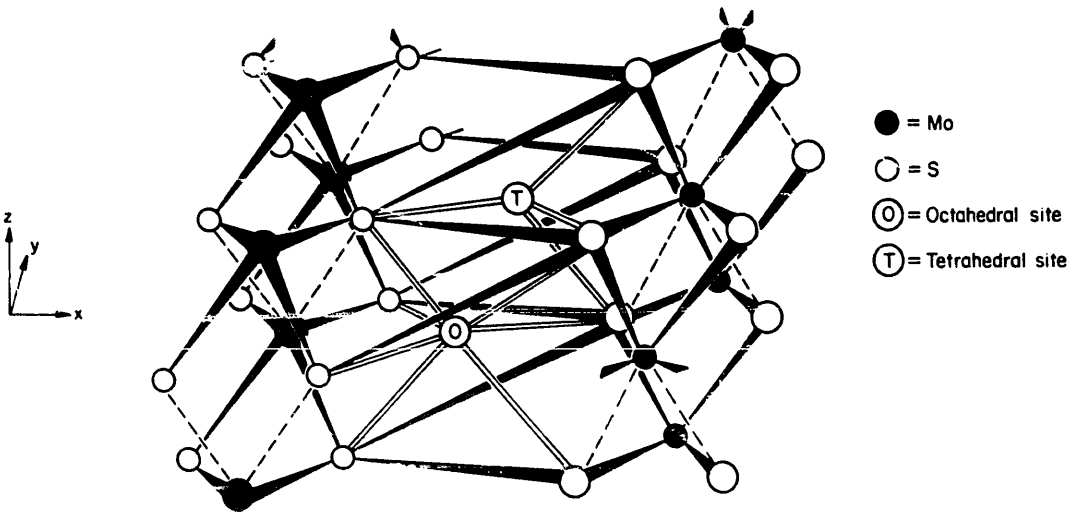

Scheme 20

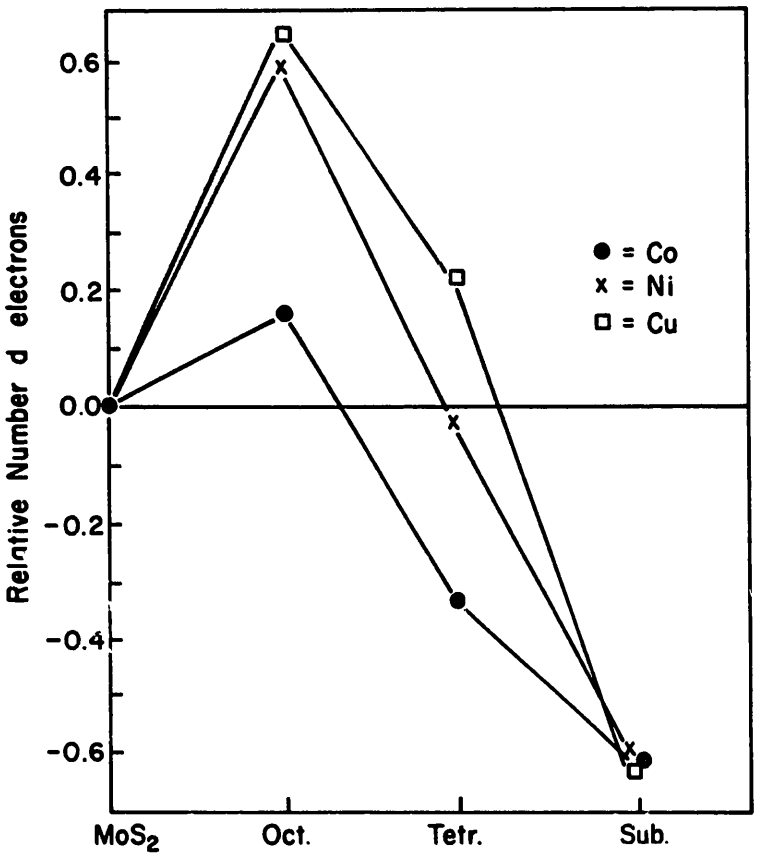

Fig. 8. Number of d electrons in protruding Mo if Co, Ni or Cu is placed in octahedral, tetrahedral or substitution sites. Value is relative to single metal MoS_2 models.

and y directions. The system of calculation is a two-dimensional slab. Co, Ni or Cu are then placed in either the octahedral or tetrahedral closest to the surface; one unit cell of each type is shown in scheme 20. At that surface, the ratio of pseudointercalate to protruding Mo and to recessed Mo is 1:1:1. Because of computational limitations, we revert to a single primitive unit cell, rather than two as for schemes 10a–10g. There remains the question as to the choice of oxidation state for the second metal. One option is to assume the oxidation state of the appropriate sulfide thought to be stable under reactor conditions, i.e. Co_9S_8, Ni_3S_2 or CuS [25]. Often, however, the identification of the second phase is ambiguous or complicated by the presence of multiple phases. The choice may also predispose the calculations for substitution at a high sulfur coordination site. To avoid such a bias, a zero oxidation state is assumed. Our results will naturally be dependent on this choice, as well as our choice of EH parameters for the second metal.

In fig. 8, the number of d electrons in the protruding Mo is plotted relative to the value computed for the one- or two-dimensional MoS_2 model for

pseudointercalation or substitution site respectively. The total Mo occupations follow very similar curves. Placement of Co, Ni or Cu in the octahedral holes always causes electronic reduction of the surface Mo 3.58 Å away, i.e. electron transfer proceeds towards Mo. The gain is specifically in x^2-y^2 and xz. The levels are redistributed such that Mo d character is lost from the S p block, but is outweighed by a gain in the lower end of the Mo d block, below ϵ_f. The governing factors are difficult to identify, but it is reasonable that the new S–pseudointercalate interaction, 2.42 Å away, reduces the number of S levels available to Mo–S_{surf} bonding and weakens the Mo–S_{surf} bonds. The d levels of Co, Ni and Cu fall in the middle of the S p block. The Co–S_{surf} o.p. is 0.252, for example. Fewer Mo levels are pulled down into the S p area, and fewer pushed up out of the Mo d block into the antibonding counterparts. Tetrahedral pseudointercalation of Cu at a distance of 4.07 Å reduces Mo, whereas the two promoters are oxidizing agents. The primary charge transfer occurs into (for Cu) or out of (for Co and Ni) the Mo xz. At neither pseudointercalation site does the electron transfer modify the Mo–Mo surface interaction; the Mo–Mo o.p. remain within 0.005 of that computed for the all Mo system.

Substitution always oxidizes the adjacent Mo, i.e. electron transfer occurs out of Mo. The strength of the metal–metal interaction is most apparent in the x^2-y^2 and yz levels, which will participate in σ and π bonding respectively. The levels are distinctly split into the bonding combinations below ϵ_f and the antibonding one above. As the d levels of Mo lie above those of Co, Ni and Cu, the mixing is unequal and more of the Mo d levels are pushed up. The mixing between the x^2-y^2 levels is so severe that a more 15% remain below 0 eV.

If the number of Mo d electrons (or total Mo charge) determines the activity of nearby sites, then these results suggest that the choice between poisoning and promotion may be simply a matter of the location of the second metal. We could speculate that atoms which promote HDS, such as Co or Ni, prefer octahedral pseudointercalation sites, whereas Cu favors substitution sites. Unfortunately, our method does not allow for a comparison of the energies of these two processes.

To directly test HDS activity of the bimetallic systems, the unit cell of scheme 6 will be used for the substitution site. The ratio of thiophene to second metal will be 1:1. For the pseudointercalation sites the unit cell dimensions in the y direction must be doubled so as to avoid adsorbate – adsorbate interactions. The two primitive unit cells in scheme 20 form the new unit cell. The translation in the x direction is removed for reasons of computational economy. The full system can be depicted as two parallel infinite ribbons, with a ratio of second metal to protruding Mo to recessed Mo of 1:2:2. η^5-thiophene coordination was examined on four bimetallic systems. The ring was placed over the Mo nearest the octahedral or tetrahedral

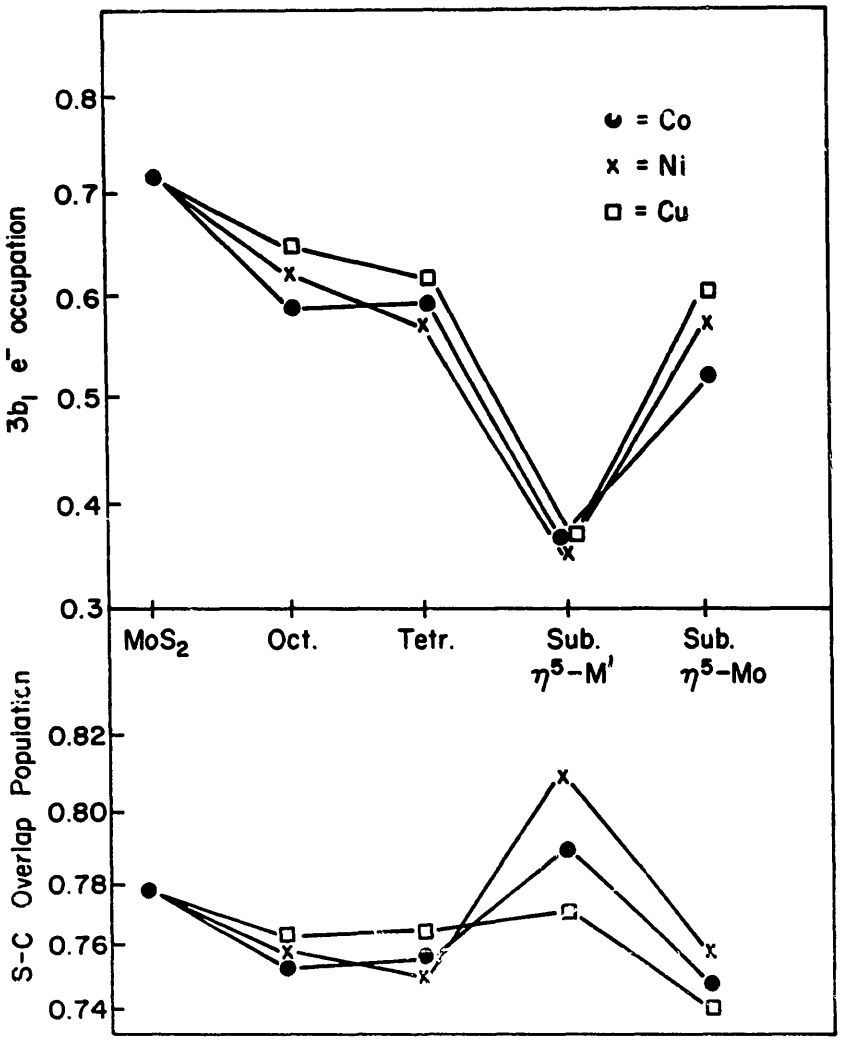

Fig. 9. For η^5-thiophene modes, the $3b_1$ occupation and S–C o.p. if Co, Ni or Cu is placed in the octahedral, tetrahedral or substitution sites. For the latter, the coordination can be over the Mo or the second metal.

metal, and alternately over either the Mo or second metal in the case of substitution. The $3b_1$ occupation and the S–C o.p. are plotted in fig. 9.

In the case of substitution when thiophene coordinates directly to Co, Ni or Cu, reduced S–C activity is observed through the elevated S–C o.p. in fig. 9. Although direct participation of Co as a promoter had been suggested on the basis of Mössbauer data [51], these results argue against such participation. The $3b_1$ occupation is strongly reduced and the S–C bond strength increases for these systems relative to η^5 coordination on the all Mo surface, scheme 10f. As is expected for later transition metals, the d blocks of Co, Ni, and Cu lie below that of Mo (see H_{ii} in table 5). The second metal d levels are in fact contained in the S p block, well below ϵ_f. With a minimum occupation of 90%

it is evident that for these 3d metals, the number of d electrons available at a site does not by itself determine the activity. The large energy difference between the d levels at -13 to -14 eV and thiophene $3b_1$ at -7.78 eV eliminates a strong backbonding interaction.

The results for the remaining three geometries are less clear cut. Although antiparallel trends are expected in the $3b_1$ occupation and the S–C o.p., the S–C bond strength is not governed solely by the extent of backbonding into $3b_1$. This is evident in these three cases, where the S–C bond weakening (decreased S–C o.p.) is not mirrored by an increase in the $3b_1$ occupation. In the all Mo model, x^2-y^2 couples most strongly with $3b_1$ (fig. 3), and the overriding factor determining the donor capacity of the metal is the strength of this Mo–$3b_1$ interaction. Although octahedral pseudointercalation brings about electron transfer into this x^2-y^2 level, it does not result in increased donation into $3b_1$. In the particular case of octahedral pseudointercalation, the presence of the second metal pushes Mo x^2-y^2 below ϵ_f. The energy difference between $3b_1$ and x^2-y^2 widens and the interaction between the two orbitals weakens. Therefore, even though the addition of the pseudointercalate results in the reduction of the surface Mo, it does not make Mo a better donor. Instead, all of the bimetallic systems are superior electron acceptors. Interactions with both sulfur lone pairs are enhanced, resulting again from the downward shift of the d levels. Although $2b_1$ is non-bonding between S and C, $9a_1$ is somewhat bonding. An average loss of $1/4$ e^- is observed for the $9a_1$ orbital; this loss may be associated with the calculated S–C bond weakening.

Although the results for the bimetallic systems provide us with some insight into how the electronic structure of the surface Mo's is altered by a pseudointercalated or substituted metal, they do not enable us to determine what type of site is optimum for the 3d metal. Although the effect on the surface Mo depends on where the 3d metal is located, the effect on the thiophene bound to a surface Mo is similar for all three locations of the 3d metal. It is particularly interesting to note, however, that even when the surface Mo's are reduced, they do not necessarily become better donors. Also, the results do suggest that a 3d metal substituted for a surface Mo does not directly provide an active site. Clearly, this is a very complex system and these results are dependent on and limited by our choice of substrate models, adsorption sites and calculation parameters. Because the system is so complex, information obtained from experiments aimed at a better characterization of both the active surface and the position of promoters or poisons will be invaluable to future theoretical efforts.

9. Conclusions

The electronic factors governing thiophene HDS on MoS_2 are complex and depend on the exact nature of the substrate and the coordination geometry of

the thiophene. As the industrial products are mainly four-membered carbon species and H_2S, and as atomic surface sulfur is frequently encountered alongside hydrocarbon fragments in clean transition metal surface investigations, we monitor the HDS process theoretically mainly through the extent of S–C bond weakening as calculated at various sites. If the model of the substrate is simply a flat Mo exposing surface, the mechanism of S–C breakage for on-top or bridging η^1- or η^5-like modes is straightforward. Occupation of the $3b_1$ thiophene orbital will weaken the bond as it is S–C antibonding. The strongest HDS activity is found in the η^5 coordination. If the thiophene adopts an η^2 mode, and H_α is lost in the process, the S–C bonding nature of the emergent carbon lone pair is of paramount importance to the bond severing. If instead, hydrogenation occurs, α-addition is energetically favored over –addition, and α-addition causes clear S–C bond weakening. Both η^2 coordination and α-hydrogenation weaken only one S–C bond, indicative of a two-step ring desulfurization mechanism.

Some type of surface defects can aid the process. For instance, the removal of a nearby surface sulfur will increase the reactivity of sites which are already preferred, such as η^5-thiophene. Activation of the η^1 site remains unchanged, although is may become a better site for initial adsorption. If some bond contraction is allowed, replacement of the thiophenic for a surface sulfur will induce some S–C weakening. It is the only S-coordinated thiophene examined which shows signs of activity. On the other hand, simple surface reconstruction by pairwise distortions of Mo or S, even if energetically favorable in itself, does not promote HDS. The introduction of a second metal, such as Co, Ni or Cu can either promote or poison the reactivity. η^5 coordination directly to any of the three will decrease HDS activity. Pseudointercalation of the second metal can induce S–C weakening via a decreased occupation of the slightly S–C bonding $9a_1$ thiophene orbital.

Clearly many aspects of the rich chemistry of HDS have yet to be explored. Because of the complexity of the system, we have examined only few simple cases. More experimental information is needed, particularly a more detailed description of the catalytic surface. And more theoretical work is needed to understand the experimental results. The richness and variety of the HDS system make it highly amenable to a strong cooperation between theory and experiment.

Acknowledgments

We thank Cynthia Friend for communicating results prior to publication and Susan Jansen for the many helpful discussions during the course of this work. The comments of the two referees were also helpful. This work was supported by the Office of Naval Research.

Table 5
Extended Hückel parameters

Orbital	H_{ii} (eV)	ζ_1	ζ_2	C_1 [a]	C_2 [a]
Mo 5s	−8.34	1.96			
5p	−5.24	1.90			
4d	−10.50	4.54	1.9	0.5899	0.5899
Co 4s	−9.21	2.00			
4p	−5.29	2.00			
3d	−13.18	5.55	2.1	0.5679	0.6051
Ni 4s	−9.17	1.83			
4p	−5.15	1.13			
3d	−13.49	5.57	2.0	0.5683	0.5744
Cu 4s	−11.40	2.20			
4p	−6.06	2.20			
3d	−14.00	5.75	1.9	0.5899	0.5899
S 3s	−20.00	1.82			
3p	−13.30	1.82			
C 2s	−21.40	1.63			
2p	−11.40	1.63			
H 1s	−13.60	1.30			

[a] Contraction coefficients used in double ζ expansion

Appendix

The extended Hückel tight binding method [27] was used throughout. The H_{ii}'s were taken from previous work and are listed in table 5 [52]. Crystal structure data was used for the geometry of the MoS_2 models [53]. The thiophene geometric parameters are [54]: $d(S-C_\alpha) = 1.723$ Å, $d(C_\alpha-C_\beta) = 1.360$ Å, $d(C_\beta-C_\beta) = 1.430$ Å, $d(C-H) = 1.079$ Å, $\angle C_\alpha-S-C_\alpha 1.7°$, $\angle S-C_\alpha-C_\beta = 111.6°$, $\angle C_\alpha-C_\beta C_\beta = 112.3°$, $\angle S-C_\alpha-H = 119.2°$, $\angle C_\alpha-C_\beta-H = 123.9°$. Thiophene was placed on one side of the unit cells. Average properties were calculated over ten and five k points respectively for the one- and two-dimensional systems [55].

References

[1] (a) B.C. Gates, J.R. Katzer and G.C.A. Schuit, Chemistry of Catalytic Processes (McGraw-Hill, New York, 1974) p. 390–426;
(b) O. Weissner and S. Landa, Sulfide Catalysts: The Properties and Applications (Pergamon, Oxford, 1973);
(c) R.R. Chianelli, Catalysis Rev.-Sci. Eng. 26 (1984) 361;
(d) E.E. Donati, Advan. Catalysis 8 (1956) 39.
[2] (a) T.A. Pecoraro and R.R. Chianelli, J. Catalysis 67 (1981) 430;
(b) J.P.R. Vissers, C.K. Groot, E.M. van Oers, V.H.J. de Beer and R. Prins, Bull. Soc. Chim. Belges 93 (1984) 813.

[3] J.M.J.G. Lipsch and G.C.A. Schuit, J. Catalysis 15 (1969) 179.
[4] M. Salmeron, G.A. Somorjai, A. Wold, R.R. Chianelli and S.K. Lang, Chem. Phys. Letters 90 (1983) 105.
[5] (a) T. Tanaka and T. Okuhara, J. Catalysis 78 (1982) 155;
(b) T. Tanaka and T. Okuhara, in: Proc. Climax IIIrd Intern. Conf. on the Chemistry of Molybdenum, Eds. H.F. Gray and P.C.H. Mitchell, (Climax Mo. Co., Ann Arbor, 1979) p. 170.
[6] S.J. Tauster, T.A. Pecoraro and R.R. Chianelli, J. Catalysis 63 (1980) 515.
[7] B.G. Silbernagel, T.A. Pecoraro and R.R. Chianelli, J. Catalysis 78 (1982) 380.
[8] D.C. Johnston, B.G. Silbernagel, M. Daage and R.R. Chianelli, in: Abstracts of the 198th ACS National Meeting, Maimi, 1985, paper PETR 76.
[9] S. Kasztlen, H. Toulhoat, J. Grimblot and J.P. Bonnelle, Bull. Soc. Chim. Belges 93 (1984) 807; Appl. Catalysis 13 (1984) 127.
[10] S. Brunauer, P.H. Emmett and E. Teller, J. Am. Chem. Soc. 60 (1938) 309.
[11] See for example:
(a) J. Bachelier, M.J. Tilliette, J.C. Duchet and D. Cornet, J. Catalysis 76 (1982) 300;
(b) F.E. Massoth, Advan. Catalysis 27 (1978) 265.
[12] C.B. Roxlo, M. Daage, A.F. Ruppert and R.R. Chianelli, J. Catalysis 100 (1986) 176.
[13] M.H. Farais, A.J. Gelman, G.A. Somorjai, R.R. Chianelli and K.S. Liang, Chem. Phys. Letters 90 (1982) 105.
[14] J.L. Roberts and C.M. Friend, Surface Sci. 186 (1987) 201.
[15] J. Stöhr, J.L. Gland, E.B. Kollin, R.J. Koestner, A.L. Johnson, E.L. Muetterties and F. Sette, Phys. Rev. Letters 53 (1984) 2161.
[16] J.F. Lang and R.I. Masel, Surface Sci. 183 (1987) 44.
[17] F. Zaera, E.B. Kollin and J.L. Gland, to be published.
[18] F. Zaera, E.B. Kollin and J.L. Gland, Surface Sci. 184 (1987) 75.
[19] E.L. Muetterties, R.M. Wexler, T.M. Gentle, K.L. Shanahan, D.G. Klarup, A.L. Johnson, V.H. Grassian, K.B. Lewis, T.G. Rucker and R. Lum, to be published.
[20] J.T. Roberts and C.M. Friend, to be published.
[21] (a) C.G. Kuehn and H. Taube, J. Am. Chem. Soc. 98 (1976) 689;
(b) N. Kuhn and H. Schumann, J. Organomet. Chem. 276 (1984) 55;
(c) M. Draganjac, C.J. Ruffing and T.B. Rauchfuss, Organometallics 4 (1985) 1909.
[22] (a) E.O. Fischer and K. Öfele, Chem. Ber. 91 (1958) 2395;
M.F. Baily and L.F. Dahl, Inorg. Chem. 4 (1965) 1306;
(b) H. Singer, Organomet. Chem. 9 (1967) 135;
D.A. Lesch, J.W. Richardson, R.A. Jacobson and R.J. Angelici, J. Am. Chem Soc. 106 (1984) 2901;
(c) C.C. Lee, M. Iqbal, U.S. Gill and R.G. Sutherland, J. Organomet. Chem. 288 (1985) 89;
(d) G.H. Spies and R.J. Angelici, J. Am. Chem. Soc. 107 (1985) 5569;
(e) S.C. Huckett and R.J. Angelici, private communication.
[23] (a) G.H. Spies and R.J. Angelici, to be published;
(b) D.A. Lesch, J.W. Richardson, R.A. Jacobson and R.J. Angelici, J. Am. Chem. Soc. 106 (1984) 2901;
(c) S.C. Huckett, N.N. Sauer and R.J. Angelici, Organometallics 6 (1987) 591;
(d) J.W. Hachgenei and R.J. Angelici, Angew. Chem., in press.
[24] (a) M. Zdražil and J. Sedláček, Collection Czech. Chem. Commun. 42 (1977) 3133;
(b) Ch. Vladov, M. Neshev, L. Petrov and D. Shopov, in: Proc. Vth Intern. Symp. on Heterogeneous Catalysis, Part II; Varna, 1983, p. 479;
(c) J. Joffre, P. Geneste and D.A. Lerner, J. Catalysis 97 (1986) 543.
[25] S. Harris and R.R. Chianelli, J. Catalysis 86 (1984) 400;
S. Harris, Chem. Phys. 67 (1982) 229.

[26] A.B. Anderson, Z.Y. Al-Saigh and W.K. Hall, to be published.
[27] (a) R. Hoffmann, J. Chem. Phys. 39 (1963) 1397;
R. Hoffmann and W.M. Lipscomb, J. Chem. Phys. 36 (1962) 3179; 37 (1962) 2872;
(b) J.H. Ammeter, H.-B. Bürgi, J.C. Thibeault and R. Hoffmann, J. Am. Chem. Soc. 100 (1978) 3686.
[28] Agreement between the one- and two-dimensional MoS_2 systems is generally within 0.005 e^- for atomic charges, 0.005 for overlap population and 0.05 eV for the Fermi energy.
[29] (a) M. Kertesz and R. Hoffmann, J. Am. Chem. Soc. 106 (1984) 3453;
(b) A.D. Yoffe, Chem. Soc. Rev. 5 (1976) 51;
(c) D.W. Bullett, J. Phys. C11 (1978) 4501; the close agreement should be considered fortuitous;
(d) R. Coehoorn, C. Haas, J. Dijkstra and A. Wold, Phys. Rev. B35 (1987) 6195, 6203.
[30] S. Harris, Polyhedron 5 (1986) 151.
[31] G. Blyholder, J. Phys. Chem. 68 (1964) 2772.
[32] (a) M.C. Zonnevylle and R.R. Hoffmann, Langmuir 3 (1987) 452;
(b) S.-S. Sung and R. Hoffmann, J. Am. Chem. Soc. 107 (1985) 578.
[33] J.C.J. Bart and V. Ragaini, in: Proc. Climax IIIrd Intern. Conf. on the Chemistry of Molybdenum, Eds. H.F. Gray and P.C.H. Mitchell, (Climax Mo. Co., Ann Arbor, 1979) p. 19.
[34] M. Gerloch and R. Mason, J. Chem. Soc. (1965) 296.
[35] (a) P.J. Hay, J.C. Thibeault and R. Hoffmann, J. Am. Chem. Soc. 97 (1975) 4884;
(b) S. Shaik, R. Hoffmann, R. Fisel and R.H. Summerville, J. Am. Chem. Soc. 102 (1980) 4555.
[36] The geometry was excised from scheme 10a. The -4 charge is achieved via the assignment of a formal oxidation state of Mo(IV) and S_2^{2-} in MoS_2. The orbital mixing arguments hold regardless of the charge assignment to the fragment.
[37] S. Harris and R.R. Chianelli, J. Catalysis 98 (1986) 17.
[38] (a) C.J. Wright, C. Sampson, D. Fraser, R.B. Moyes, P.B. Wells and C. Reikel, J. Chem. Soc. Faraday Trans. I, 76 (1980) 1585;
(b) W.K. Hall and W.S. Millman, in: Proc. 7th Intern. Congr. on Catalysis, B, Tokyo, 1980, p. 1304;
(c) P. Ratnasamy and J.J. Fripiat, Trans. Faraday Soc. (1970) 2897.
[39] P. Pokorný and M. Zdrazil, Collection Czech. Chem. Commun. 46 (1981) 2185.
[40] W.S. Yang, F. Jona and P.M. Marcus, Phys. Rev. B28 (1983) 2049.
[41] M. Boudart, Progr. Chem. Eng. 57 (1961) 33.
[42] C. Wivel, R. Candia, B.S. Clausen, S. Mørup and H. Topsøe, J. Catalysis 68 (1981) 453.
[43] R.J.H. Voorhoeve and J.C.M. Stuiver, J. Catalysis 23 (1971) 236, 243.
[44] A.L. Farragher and P. Cossee, in: Proc. Vth Intern. Congr. on Catalysis, Palm Beach, 1972, Ed. J.W. Hightower (North-Holland, Amsterdam, 1973) p. 1301.
[45] R.R. Chianelli, A.F. Ruppert, S.K. Behal, B.H. Kear, A. Wold and R. Kershaw, J. Catalysis 92 (1985) 56.
[46] H. Topsoe, B.S. Clausen, R. Candia, C. Wivel and S. Mørup, J. Catalysis 61 (1981) 433.
[47] (a) P. Grange and B. Delmon, J. Less-Common Metals 36 (1974) 353;
(b) G. Hagenbach, Ph. Courty and B. Delmon, J. Catalysis 31 (1973) 264.
[48] F. Delanney, D.S. Thaker and B. Delmon, J. Less-Common Metals 63 (1979) 365.
[49] See for example;
(a) G.C.A. Schuit and B.C. Gates, Am. Inst. Chem. Eng. J. 19 (1973) 417;
(b) P.R. Wentrcek and H. Wise, J. Catalysis 45 (1976) 349;
(c) R.W. Phillips and A.A. Fote, J. Catalysis 41 (1976) 163;
(d) B. Delmon, in: Proc. Climax IIIrd Intern. Conf. on the Chemistry of Molybdenum, Eds. H.F. Gray and P.C.H. Mitchell (Climax Mo. Co., Ann Arbor, 1979) p. 73.

[50] R.R. Chianelli, T.A. Pecoraro, T.R. Halbert, W.-H. Pan and E.I. Stiefel, J. Catalysis 86 (1984) 226.
[51] B.S. Clausen, S. Mørup, H. Topsøe and R. Candia, J. Phys. (Paris) 37 (1976) C-6;
S. Mørup, B.S. Clausen and H. Topsøe, J. Phys. (Paris) 40 (1979) C-2.
[52] R.H. Summerville and R. Hoffmann, J. Am. Chem. Soc. 98 (1976) 7240;
J.W. Lauher, M. Elain, R.H. Summerville and R. Hoffmann, J. Am. Chem. Soc. 98 (1976) 3219;
K. Tatsumi and R. Hoffman, Inorg. Chem. 20 (1981) 3771.
[53] R.W.G. Wyckoff, Crystal Structures, Vol. 1, 2nd ed. (Wiley, New York, 1963) p. 280.
[54] B. Bak, D. Christensen, J. Rastrup-Andersen and E. Tannenbaum, J. Chem. Phys. 25 (1956) 890.
[55] J.D. Pack and H.J. Monkhorst, Phys. Rev. B16 (1977) 1748.